Impact of warming on rainfall changes in damaging Philippine typhoons using high-resolution convection-permitting models~~Changes in tropical cyclone associated precipitation of highly damaging Philippine typhoons using high-resolution PGW simulations and multiple-experiment approach~~

Rafaela Jane Delfino[1,2,3*]; Gerry Bagtasa[1,3]; Pier Luigi Vidale[2,4]; Kevin Hodges[2,4]

[1] Institute of Environmental Science & Meteorology, University of the Philippines - Diliman, Quezon City, Philippines
[2] Department of Meteorology, University of Reading, Reading, United Kingdom
3 Natural Science Research Institute, University of the Philippines - Diliman, Quezon City, Philippines
[4] National Center for Atmospheric Sciences, Reading, United Kingdom

* *Correspondence to*: Rafala Jane Delfino (rdelfino@iesm.upd.edu.ph)
ORCID ID: Rafaela Jane Delfino 0000-0001-8612-0342; Pier Luigi Vidale 0000-0002-1800-8460; Gerry Bagtasa 0000-0002-5433-7122

Abstract. This study has investigated the changes in tropical cyclone (TC)-associated precipitation in the Philippines under past (pre-industrial) and future climate scenarios using the pseudo-global warming technique and dynamical downscaling. ~~What is novel~~The novelty ~~in~~ of this work is in the use of high-resolution PGW simulations (3km and 5km) and a multiple-experimental approach to directly quantify TC precipitation changes over the Philippines, as well as the decomposition of TC rainfall changes in thermodynamic and dynamic contributions.~~revealing the nonlinear response of precipitation scaling to different warming pathways. F~~Future climate simulations project a significant increase in TC precipitation, consistent with Clausius-Clapeyron (CC) scaling expectations. However, small deviations from this expected scaling are noted, attributed to factors such as increased TC intensity and atmospheric warming. The simulated TC precipitation in the past climate is found to be lower than that in the current climate, with inner-core precipitation increases of ~6–8% from past to present conditions.~~. Our convection-permitting model experiments estimate that the average TC inner-core precipitation rate changes from past to current climate conditions are 6% and 8% for the 5km and 3km, respectively. Under the SSP5-8.5 future scenario, simulations indicate a robust rise (by approximately 6% per 1K increase in SST relative to the current climate) in the mean precipitation rates for intense TCs such as Haiyan (2013), Bopha (2012), and Mangkhut (2018) in both the 5km and 3km experiments. Notably, simulations that warm only land and sea surfaces show increases exceeding CC expectations, reaching up to 13% per 1K increase in SST. Increases in both radial and vertical extent of rain are observed. Our analysis shows that these changes are linked to enhanced latent heating, moisture, and updrafts in the TCs' inner-core regions, emphasizing intricate interactions between~~

~~atmospheric processes and the evolving structure of TCs.~~ Under future warming (SSP5-8.5), simulations indicate robust increases in TC rainfall rates for intense TCs such as Haiyan (2013), Bopha (2012), and Mangkhut (2018), with strongest amplification in the inner-core region. Extreme rainfall increases disproportionately (locally exceeding 30–40%), indicating a shift toward short-duration, high-intensity rainfall events rather than uniform rainfall enhancement. However, our results show that this increase is primarily driven by thermodynamic effects (≈20–30%), while dynamical contributions are smaller (≈−10% to −30%) and often partially offset the total rainfall response. Overall, the results demonstrate that TC rainfall scaling in a warming climate is primarily moisture-driven, with TC case-to-case dynamics modulating the TC associated rainfall response. Our study underscores that variations in TC intensity and structure play a crucial role in influencing the scaling relationship between sea surface temperatures and TC-associated precipitation in the Philippines.

Keywords: tropical cyclones, precipitation, Philippines, global warming, Clausius-Clapeyron scaling

1. Introduction

Tropical cyclones (TCs) make significant rainfall contributions in the Philippines (Bagtasa, 2017; 2022) and are a ~~key~~ major source of freshwater (Ribera *et al*., 2005; Kubota & Chan, 2009; Yumul *et al*., 2012). The study of Kubota and Wang (2009) and Bagtasa (2017) showed that TC-induced precipitation (determined over a radial distance of 1000 km from TC centers) in certain regions of the Philippines contributes to more than 50% of the annual total precipitation. TC precipitation rates are projected to increase with global warming, which will consequently exacerbate TC-associated floods and landslide risks (Knutson *et al*., 2021; Kossin, 2018; Liu *et al*., 2019). The Intergovernmental Panel on Climate Change (IPCC) 6th Assessment Report (AR6) has concluded that it is very likely that average TC rain rates will increase with warming, and peak TC rainfall rates will likely exceed the Clausius-Clapeyron scaling (CCS) rates in some regions (IPCC 2021). In a multi-model assessment, Knutson et al. (2020) projected that TC rainfall could increase globally by +6% to +22% under +2°C warming. In the Western North Pacific (WNP) Basin, increases of +5% to +7% per °C are consistently reported (~~Wang et al., 2014; 2015~~Lee et al., 2020). Furthermore, an assessment by the Economic and Social Commission for Asia and the Pacific (ESCAP)/ World Meteorological Organization (WMO) ~~ESCAP/WMO~~ Typhoon Committee (Cha et al., 2020) found a median increase of 17% in TC precipitation rates, with a 10th–90th percentile range of +6% to +24% in the WNP.

The CCS is commonly used to describe the relationship between air temperature and moisture-bearing capacity of air - about 7% more water vapor per 1°C of warming - leading to higher rainfall potential in a warmer world (Trenberth et al., 2007; Allen & Ingram, 2002; Held & Soden, 2006). However, TC-associated precipitation may increase at higher rates per degree change in temperature due to dynamical processes, such as increased latent heat fluxes and stronger convergence, which amplify rainfall beyond the thermodynamic expectations (Shi et al., 2024). Empirical studies have supported the application of CCS in explaining increases in TC precipitation (Trenberth et al., 2007; Vecchi et al., 2008). Nonetheless, regional discrepancies have been observed. Kossin et al. (2017) and O'Gorman (2020) noted that observed precipitation changes in certain regions deviate from CCS, likely due to TC dynamics, moisture transport, and local atmospheric circulation.

Recent studies have explored ~~Recently, as a result, the~~ concept of Super-CCS has emerged in literature, referring to rainfall increases that exceed the expected 7% per °C ~~threshold~~ of CCS. For example, Liu et al. (2019) reported that average rainfall rates within a 100-km radius from the center ~~for~~ of TCs with tropical storm intensity could increase by 13%–17% per °C under 21st-century warming. Huprikar et al. (2024) also found that future rainfall associated with Hurricane Irma exceeded CCS expectations. These findings suggest that TC inner-core intensification and structural changes, such as vertical expansion of the eyewall and enhanced updraft, play a critical role in amplifying precipitation beyond the CCS rate. Despite these findings, there is still a limited understanding of whether TC-associated rainfall in the Philippines conforms to CCS or exhibits Super-CCS properties, especially under changing climate conditions where TCs are projected to intensify (Delfino et al., 2023; 2024). While previous studies have examined TC intensity and precipitation changes (Villarini et al., 2014; Patricola & Wehner, 2018; Liu et al., 2019; Xi et al., 2023), detailed analyses that isolate rainfall scaling with warming remain sparse. Recent work by Yang and Toumi (2025) highlighted that the changes in TC rain due to

Formatted: Superscript

Formatted: Not Highlight

global warming may arise through at least two distinct pathways: thermodynamic effects associated with the increased atmospheric moisture holding capacity and enhanced latent energy availability, and through dynamic effects associated with changes in TC circulation and vertical motion. Distinguishing between these two is important since thermodynamic forcing may yield very different rainfall characteristics depending on the TC structure and dynamics. As a result, CC scaling alone may not adequately represent event-scale changes in TC rainfall hazards. However, most previous studies have relied on basin-scale composites or coarse-resolution models, and even fewer studies have examined whether the CC scaling hold, and which pathway, applies for individual high-impact TCs in convection-permitting simulations. This study aims to fill this gap by ~~analyzing~~analysing three highly damaging Philippine TCs - Haiyan (2013), Bopha (2012), and Mangkhut (2018) - ~~using convection-permitting model simulations~~ under pre-industrial, present, and future climates. Applying the pseudo-global warming (PGW) technique, we investigate:

- How does the TC-associated precipitation in the Philippines change under past and future climate scenarios, and to what extent do these changes align with the expectations of CCS?
- How do variations in TC intensity and structure influence the scaling relationship between sea surface temperatures and TC-associated precipitation in the Philippines?
- To what extent can we ascribe these precipitation changes to dynamical versus thermodynamic drivers?

Formatted: Indent: Left: 0.34", No bullets or numbering

A better understanding of these mechanisms is critical for anticipating current and future flood risks and improving disaster preparedness in the Philippines. The paper continues in Section 2 ~~of this paper discusses~~with discussion of the methods, Section 3 provides the results and discussion, and Section 4 highlights the conclusions.

2. Methods

2.1 Model Configuration

The Advanced Research Weather Research and Forecasting (WRF-ARW) model version 3.8.1 (Skamarock et al. 2008) was used to simulate TCs in the present study. The European Centre for Medium-Range Weather Forecasts (ECMWF) 5th generation Reanalysis dataset (ERA5) was utilized ~~as~~ for the initial and lateral boundary ~~forcing~~ conditions with two model domain configurations: (1) a two-way grid nesting of 25 km outer and 5km inner domains, with the Kain-Fritsch cumulus parameterization (hereafter referred to as 5kmCU) turned on, and (2) a convection-permitting (no cumulus parameterization) single domain 3-km resolution (herafter referred to as 3kmNoCU), to account for the uncertainty in the use of cumulus parametrizations. Both model configurations have 44 vertical levels and use a sigma vertical coordinate from the surface up to the top of the atmosphere at 50 hPa. The details of the other model parameterization schemes (i.e., microphysics, boundary layer, etc.) used can be found in Delfino et al., (2023).

2.2 Experimental Design

Three TC cases are selected based on the region in the Philippines where the TCs made landfall, the month of occurrence, and associated damages – Typhoons Haiyan (2013), Bopha (2012), and Mangkut (2018). More detailed information on these three TC cases is described in Delfino et al. (2023). The three TC cases were simulated with four different initialization times to create an ensemble from a single driving reanalysis, thereby minimizing uncertainties from variations in the initial conditions. For tracking the simulated TCs, the simulated track and intensity values were obtained every 6 hours using the TRACK algorithm (Hodges et al., 2017) as used in Hodges and Klingaman (2019) and Delfino et al. (2023).

Multi-model datasets from the Coupled Model Intercomparison Project phase 6 (CMIP6) (Eyring et al., 2016) were used to apply the PGW method, introduced by Schär et al. (1996)~~.~~. We simulated the TC cases under different climate conditions by primarily adjusting the following parameters: SST, atmospheric temperature, and relative humidity (RH) between current and future climate conditions. Four CMIP6 models were used~~,~~, to extract the climate change forcing,~~-~~ and results for all ensemble members were averaged for each of the CMIP6 models. The models - HadGEM3-C31-LL, CESM2, MIROC6, MPI-ESM1-2-HR – were chosen to represent different warming levels, under the Shared Socio-economic Pathways (SSP) 5-8.5 scenario. The PGW delta is calculated by subtracting the monthly means (i.e., November for Haiyan, December for Bopha, and September for Mangkhut) of the historical simulations (1970-2000) from the future projected climate (2070-2099) and the pre-industrial climate (1850-1899) ~~.~~The calculated PGW deltas for each variable (surface and ~~air~~ atmospheric temperature, surface and sea-level pressure, geopotential height, and ~~RH~~relative humidity) were then added to the 6-hourly ERA-5 initial and boundary conditions for the three TC cases to build the PGW conditions. For this study, we have included changes in relative humidity~~RH~~ to further understand its effects on TC response (referred to as FULL experiments). ~~We also performed simulations with only the SST change (SFC only) and with SFC only and 3D temperature changed (SFC+PLEV) experiments.~~ Each of the experiments and typhoon cases was initialized at 00, 06, 12, and 18 UTC. A more detailed description of the methodology can be found in Delfino et al. (2023).

Table 1. Summary of experiments

Simulation Group/Code	**Variables with PGW Delta***	**Model configuration**	**Case Study (Initial Times)**
CTRL / Current	None	5kmCU & 3kmNoCU	Haiyan (04 Nov 00, 06, 12, 18 UTC) Bopha (02 Dec 00, 06, 12, 18 UTC) Mangkhut (10 Sep 00, 06, 12, 18 UTC)
FUTURE: FULL	Surface (land and sea) temperature, air temperature, relative humidity	5kmCU & 3kmNoCU~~5kmCU~~	
PRE-INDUSTRIAL	Surface (land and sea) temperature, air temperature, relative humidity	5kmCU & 3kmNoCU	

Formatted: Left

Formatted: Left

It is also important to note here that the PGW technique faces challenges related to spin-up and dynamical balance when simulating TCs. Spin-up issues arise because the initial conditions need time to adjust to imposed future climate anomalies, potentially leading to unrealistic results during the adjustment period. Additionally, altering these conditions can disrupt the dynamic balance of the atmospheric system, resulting in inaccuracies in the intensity and behavior of simulated TCs. These issues were explored and addressed in Delfino et al., (2024).

2.3 TC precipitation analysis

2.3.1 TC precipitation rate and total accumulated precipitation

Formatted: Indent: Left: 0"

We analysed the TC precipitation rate and total accumulated precipitation during the duration of the simulations. We also investigated the relationships between TC rain rate and TC wind speed, emphasizing how this relationship varies within the TC inner-core region (2.51° distance from the center). We also analysed the simulated reflectivity rates (in dbz) from the WRF simulations and vertical profiles of the averaged composites over multiple time steps (e.g., average reflectivity during peak intensity hours) of simulated reflectivity over a 1° and 2.5° radius in the forward direction of the storms for the simulations, since TCs typically have the highest precipitation rates and strongest reflectivity in their forward quadrant due to the combined effects of TC motion and cyclonic rotation. By focusing on this region, we can capture the most intense precipitation features and better understand the TC's impact. Reflectivity is particularly useful because it provides insight into the microphysical structure of convection within TCs. Higher reflectivity values typically correspond to deeper and more intense convective cores, which are closely linked to strong updrafts and heavy rainfall production. The profiling is done at peak intensity at height levels between 0 and 18 km, and the radial grid extends to 10° for each simulation.

2.3.2 Thermodynamic and dynamic decomposition on TC rainfall changes

Following Yang and Toumi (2025), the changes in rainfall were decomposed into thermodynamic and dynamic contributions. Analysis was initially done within a 500km radius from the TC center for key rainfall metrics (as in Yang and Toumi, 2025) – azimuthally averaged maximum rainfall rate (Pm), total rainfall volume, and mean rainfall rate from each grid cells, along with rainfall intensity percentiles (P90, P95, P99). Each of these aspects of rainfall changes was then decomposed based on Yang ad Toumi (2025); the total rainfall response was partitioned into thermodynamic and dynamic contributions based on the vertical integral of ascent acting on moisture stratification. Ensemble statistics were then summarized using the median and interquartile range. Additionally, we quantified the TC wind intensity vs TC rainfall scaling based on Chen et al. (2025).

3. Results and Discussion

3.1 Changes in the total accumulated rainfall

~~The discussions in Sections 3.1 and 3.2 below are from the FULL experiments, with additional discussions on other sets of experiments in Section 3.3. Future precipitation changes in the FULL experiments reached a maximum percentage change in hourly rainfall rate of 18% (18%) for Haiyan, 11% (20%) for Bopha, and 26% (7%) for Mangkhut in the 5kmCU (3kmNoCU) runs under future climate conditions; and up to more than 18% (18%) in total accumulated precipitation over the simulation period for Typhoon Haiyan, 12% (20%) for Bopha, and 25% (7%) for Mangkhut (Figure 1). In contrast, in the simulations under pre-industrial climate conditions, TC-associated precipitation are less than the current climate, with percentage changes (pre-industrial minus current) in total accumulated precipitation over the simulation period of -3%(-2%) for Haiyan, -20%(0%) for Bopha, and -6%(-16%) for Mangkhut; and percentage change in precipitation rate of -3%(-2%) for Haiyan, -19%(0%) for Bopha, and -2%(-16%) for Mangkhut in the 5kmCU(3kmNoCU) runs (Figure 1).~~

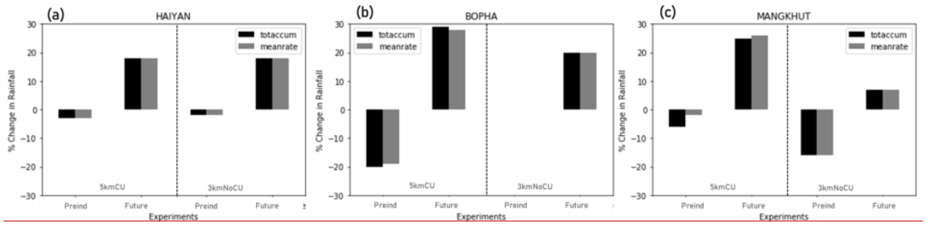

~~***Figure 1. Percent changes in total accumulated and mean precipitation rate relative to current climate for the 5kmCU runs (left panel) and the 3kmNoCU runs (right panel) under the pre-industrial and future climate relative to current climate conditions for (a) Typhoon Haiyan, (b) Typhoon Bopha, and (c) Typhoon Mangkhut***~~

~~Inspection of the time series of accumulated precipitation, along with the changes in RH, reveals that the precipitation under the future climate tends to be higher than the current, with the current climate also yields higher TC rainfall than the pre-industrial in both variables (Figure 2). Under future climate conditions, there is a consistent and notable increase in accumulated precipitation compared to the current climate. This observed rise in TC precipitation indicates a possibility of more extensive and prolonged precipitation events in the future. Furthermore, the current climate model runs exhibit higher accumulated precipitation than the pre-industrial period, reflecting an ongoing trend of changing precipitation patterns over time. Simultaneously, changes in RH are scrutinized in conjunction with the accumulated precipitation. The analysis reveals the same upward trajectory, with higher RH levels (Figure 2, right panels) in both the current and future climates compared to the pre-industrial era.~~

Figure 1 illustrates the temporal evolution of accumulated rainfall within TC-centered radii of 1.0° and 2.5° for Typhoons Haiyan, Bopha, and Mangkhut under preindustrial, present-day, and future climate. Across all TCs, accumulated rainfall increases progressively from preindustrial to current and future climates, with divergence between simulations becoming evident during the primary rainfall accumulation phase between approximately 72 and 96 hours of TC growth.

Within the 1.0° radius, future simulations consistently produce larger rainfall totals compared with present-day conditions. For Typhoon Haiyan, accumulated rainfall increases from approximately 295 mm in the preindustrial simulations to about 320 mm in the current climate and reaches roughly 365–370 mm under future warming, corresponding to an increase of approximately 14–16% relative to present-day conditions. Typhoon Bopha exhibits lower overall rainfall totals but similar behavior, with accumulation increasing from about 145 mm in the preindustrial climate to nearly 220 mm in the current climate and approximately 230–240 mm in the future simulations, representing a more modest enhancement of about 5–8% relative to current conditions. For Typhoon Mangkhut, which produces the largest rainfall totals among the three cases, accumulated rainfall increases from approximately 500 mm under preindustrial conditions to about 630 mm in the present climate and exceeds 650 mm in the future environment, equivalent to an increase of roughly 5–7%.

At the larger 2.5° radius, accumulated rainfall increases remain evident but display stronger inter-storm variability. Haiyan shows an increase from approximately 220 mm in the current climate to about 255–260 mm under future conditions, corresponding to an enhancement of roughly 15–18%. The strongest relative response occurs for Bopha, where rainfall totals increase from approximately 170 mm to nearly 230 mm, representing an increase approaching 35–40%. Mangkhut exhibits comparatively smaller fractional changes, with totals increasing from roughly 485 mm to about 505–520 mm, corresponding to increases of approximately 4–7%. Ensemble spread is largest during periods of rapid increase in precipitation volume (cumulative precipitation), particularly between 48 and 96 hours, although the ordering of rainfall totals among climate states remains consistent throughout TC lifespan.

Formatted: Indent: First line: 0"

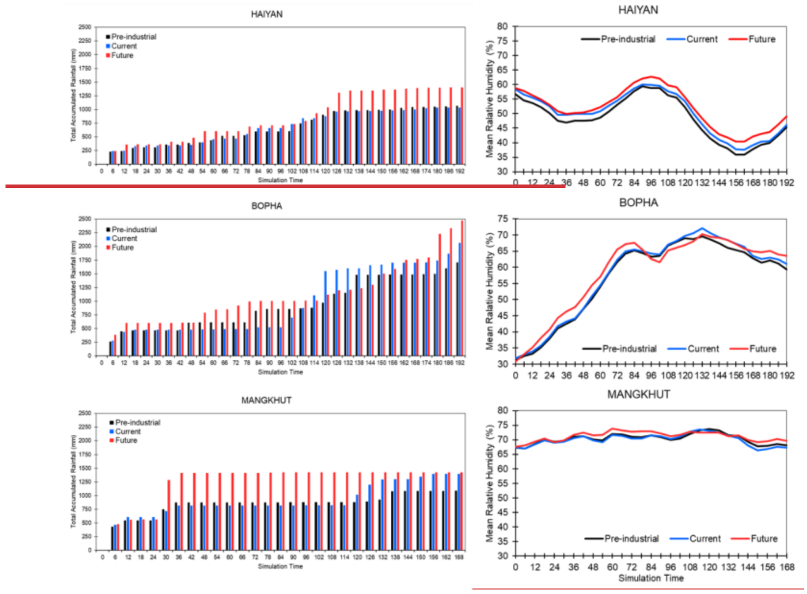

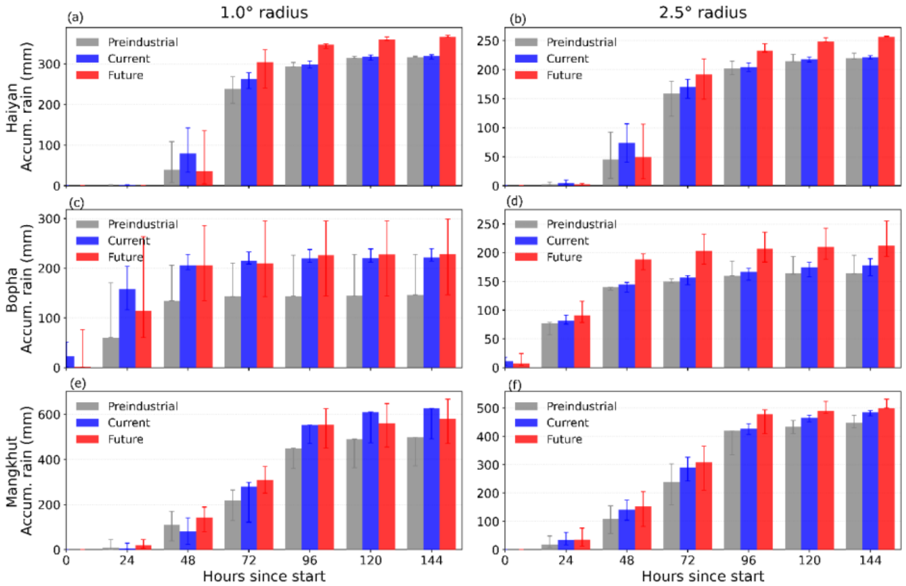

Figure 21. Total accumulated precipitation rainfall within 1.0° (left column) and 2.5° (right column) radii from the storm center for Typhoons Haiyan, Bopha, and Mangkhut under preindustrial (blue), current (gray), and future (red) thermodynamic conditions.(left panel) and mean mid-tropospheric RH (right panel) of the TC

cases under pre-industrial, current, and future climate throughout the simulation period of the three TC cases under the 5kmCU simulations.

Figure 3 2 shows the differences in total accumulated rainfall between Current minus Pre-industrial (upper panels) and Future minus Current (lower panels). Figure 3a 2 shows that there is an overall statistically significant ($p = 0.0066$) increase, particularly in the central sections of the Philippines. Bopha exhibits moderate increases across parts of Mindanao and the Visayas, with a mean significant increase of 1.7%. Mangkhut, on the other hand, shows a substantial total accumulated rainfall increase, especially over northern Luzon, with a mean increase of 14.2 mm (10.5%), statistically significant at $p < 0.0001$. For the Future minus Current plots, Haiyan shows a notable increase in rainfall in the Visayas and central Mindanao, with a mean increase of 10.1 mm (7.4%), also significant. Bopha shows the largest increase, particularly over Luzon and Visayas, with a 26.3 mm (24.3%) increase. Mangkhut, in contrast, shows a very minimal increase in rainfall over northern Luzon and surrounding regions, with a mean increase of 3.9%, primarily driven by the slight northward shift in the tracks of Mangkhut under future simulations.

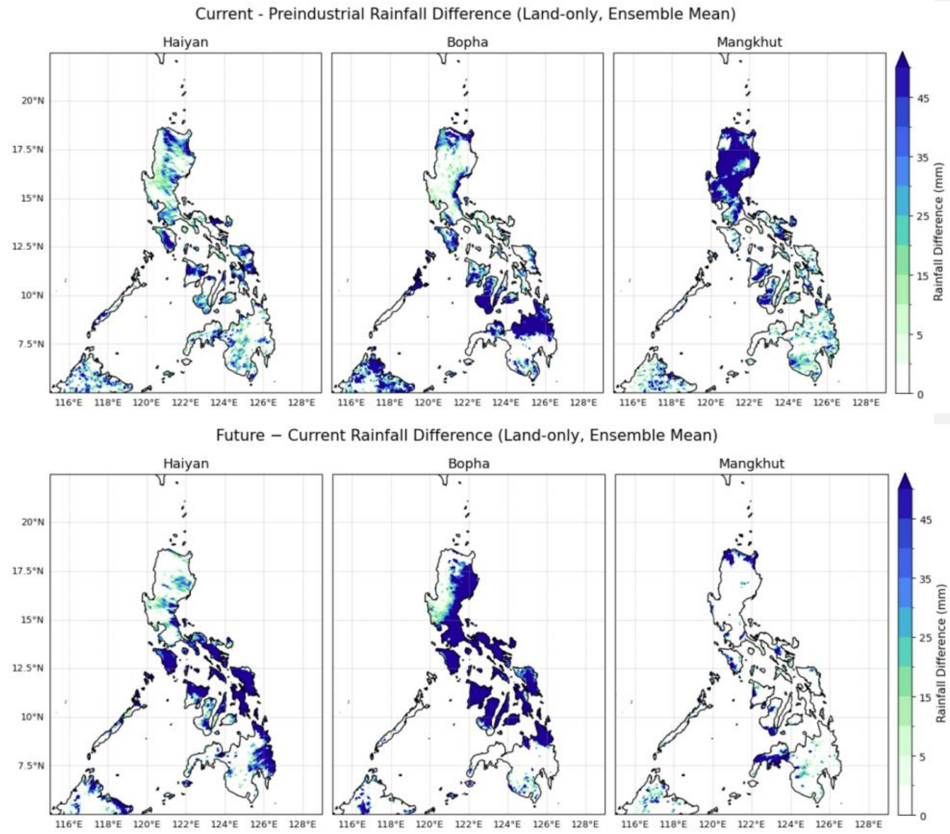

Figure ~~3~~2. Difference in the ensemble-mean accumulated precipitation (a-c, top panels) Current minus Pre-industrial; (d-f, bottom panels) Future minus Current for Typhoons Haiyan (left), Bopha (middle) and Mangkhut (right) under the 3kmNoCU simulations.

Figure 3 summarizes the total accumulated rainfall integrated over the full TC lifetime within 1.0° and 2.5° radii from the TC center. Consistent with the temporal evolution presented in Figure 1, TC-total rainfall increases systematically from preindustrial to current and future climates for all storms and spatial scales. Within the 1.0° radius, total accumulated rainfall for Haiyan increases from approximately 95 mm in the preindustrial simulations to about 110 mm in the current climate and nearly 145–150 mm in the future simulations, corresponding to an increase of roughly 30–35% relative to present-day conditions. Bopha shows an increase from approximately 85 mm to nearly 100 mm and subsequently to about 115–120 mm, representing a future enhancement of approximately 15–20%. Mangkhut exhibits the strongest relative increase within the inner-core region, with totals rising from approximately 15–20 mm in the preindustrial climate to about 25–30 mm in the current climate and reaching nearly 85–90 mm under future warming, corresponding to increases exceeding 200% relative to present-day values, although accompanied by larger ensemble variability.

At the broader 2.5° radius, rainfall totals increase across all storms, with Haiyan increasing from approximately 95 mm to about 120 mm and further to nearly 140–145 mm under future conditions. Bopha exhibits an increase from roughly 120 mm in the preindustrial simulations to approximately 165 mm in the current climate and more than 225–235 mm in the future climate, corresponding to increases of approximately 35–40%. Mangkhut increases from approximately 20 mm to about 35 mm and exceeds 100 mm under future warming, indicating substantial amplification of storm-scale rainfall accumulation.Figure 4 shows the boxplots of the distribution of total accumulated rainfall (in mm) for the three typhoons under the three climate scenarios: Preindustrial (black), Current (blue), and Future (red). This shows that both Haiyan and Bopha exhibit substantial increases in total rainfall with warming, whereas Mangkhut shows a relatively smaller increase. For Typhoon Haiyan, the ensemble median total rainfall increases in the Future scenario by approximately 9% increase. For Bopha, we are looking at approximately 23% increase from preindustrial to the future scenario, while Mangkhut exhibits minimal change. The interquartile range (IQR) also shifts upward, with higher ensemble spread under future warming for all three TCs, again with relatively minimal change for Mangkhut compared to Haiyan and Bopha. The current scenario shows little deviation from preindustrial.

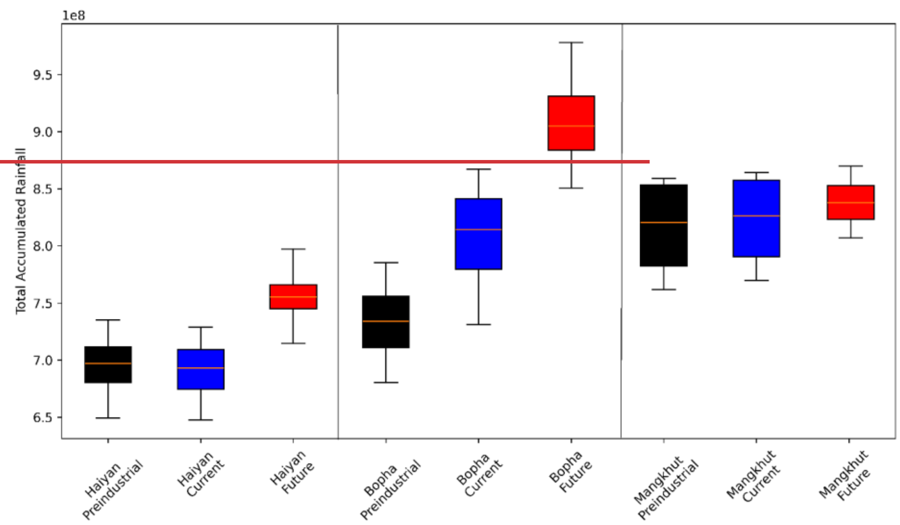

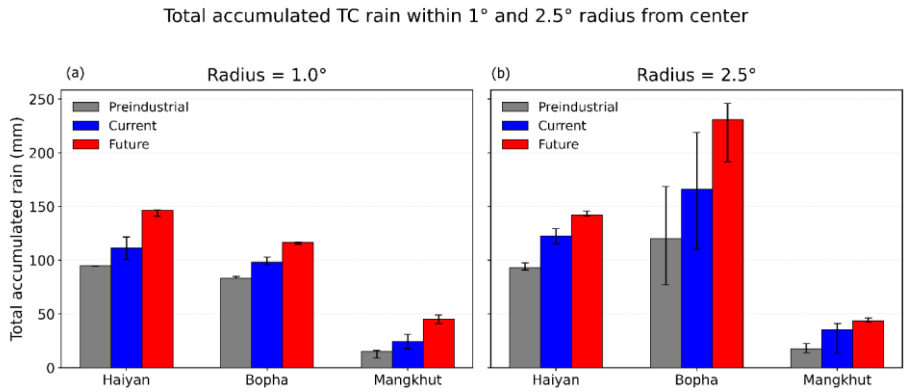

Figure 43. Boxplots for the Total Accumulated Rainfall within 1° and 2.5° radius of the center of the track from the preindustrial, current, and future climate scenarios for Typhoons Haiyan, Bopha, and Mangkhut under the 3kmNoCU simulations using all ensemble members. Error bars represent ensemble interquartile range.

3.2 Changes in TC rain rate and intensity in the simulations

Figure 4 shows that the TCs under future climate simulations consistently produce higher median rain rates and larger ensemble spread, particularly within the inner-core (1.0° radius). This indicates stronger convective variability and episodic rainfall bursts under warming, while outer-region rainfall (2.5° radius) shows comparatively modest amplification.

Formatted: Font: Not Bold, Not Italic

Formatted: Font: Not Bold, Not Italic

Formatted: Font: Not Bold, Not Italic

Across all three TC cases, projected warming leads to a systematic intensification of rainfall extremes, although the magnitude of change varies by storm and percentile threshold (Figure 4). Relative to the current climate, the future simulations show robust increases in extreme rain rates, particularly at the upper tail, indicating a disproportionate amplification of the most intense precipitation events. Haiyan exhibits the strongest sensitivity, with increases exceeding ~40% at P99, consistent with thermodynamic scaling associated with enhanced atmospheric moisture availability. In contrast, preindustrial simulations generally show reduced or weakly positive changes, especially for Bopha, suggesting that present-day rainfall extremes already reflect substantial anthropogenic influence. The asymmetric response between preindustrial cooling and future warming highlights nonlinear rainfall sensitivity to SST forcing and storm dynamics.

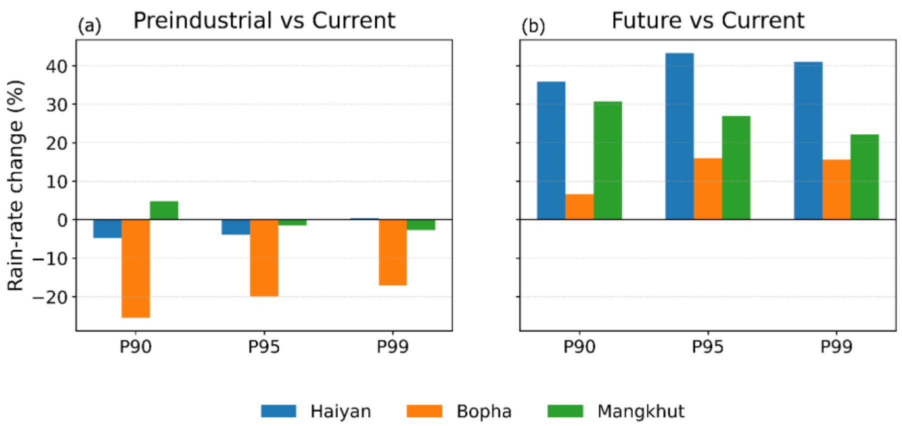

Figure 4. Percent change in rainfall intensity at the P90, P95, and P99 thresholds for Typhoons Haiyan, Bopha, and Mangkhut under (a) preindustrial and (b) future thermodynamic conditions relative to present-day simulations.

Figure 5 below shows the frequency distributions of the rainfall rates for Haiyan, Bopha, and Mangkhut across three climate scenarios (Preindustrial, Current, Future), with the left panels showing the frequency of different precipitation rates (in mm/day) and the right panels showing the distributions of the rainfall amount associated with each precipitation rate. Based on this figure, the future scenarios (red line) show a rightward extension (tail), indicating an increase in the frequency of higher rates across all TCs. Meanwhile, most total rainfall amounts (right panels) in current and future climates are in the higher end (≥100 mm/day).

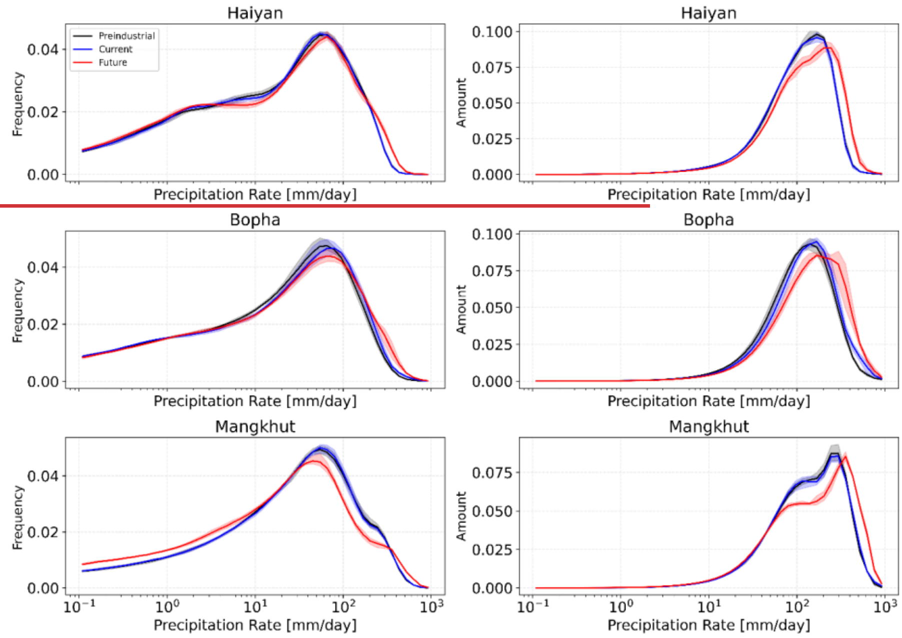

~~**Figure 5. Distributions of Typhoons Haiyan, Bopha, and Mangkhut's precipitation rate (left panels), frequencies (%), and (right panels) amounts (mm d-1) for the pre-industrial, current, and future scenarios under the 3kmNoCU simulations using all ensemble members.**~~

~~Figure 6 shows the boxplots of percent changes in mean, 95th, and 99th percentiles of 6-hourly rainfall rates for Haiyan, Bopha, and Mangkhut relative to the current climate scenario. Future simulations (red boxes) show consistently higher median percent increases, particularly for the mean rainfall across all TCs. However, the rainfall extremes (95th and 99th percentiles) increase more modestly, but in most cases, they still exceed the 7%/K baseline, suggesting potential influence from TC intensity. The figure also shows a high spread in the ensemble in terms of spread and outliers, particularly in the percent changes in mean rainfall.~~

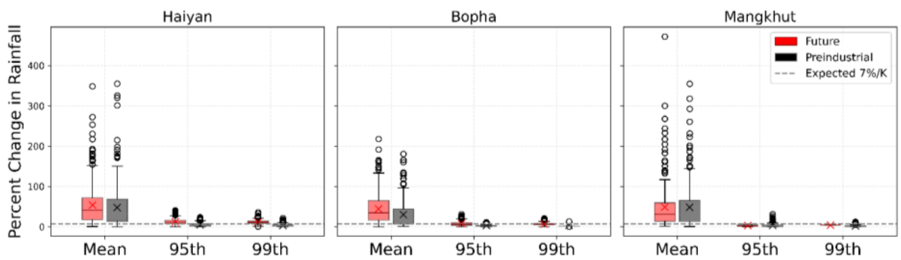

~~**Figure 6. Percent change in 6-Hourly Rainfall Rates of the Pre-industrial and Future simulations compared to Current simulations for Typhoons Haiyan, Bopha, and Mangkhut. The x-axis shows different metrics: mean 6-hourly rate, and 95th and 99th percentiles. The X markers denote the average percent change, and the black**~~

The fractional rainfall contribution analysis (Figure 5) further demonstrates that warming shifts rainfall distributions toward higher rain-rate thresholds. Under future conditions, a larger fraction of total TC rainfall originates from intense precipitation (>20–50 mm hr^{-1}), implying increasing dominance of short-duration, high-impact rainfall bursts rather than uniform TC-wide enhancement.

Formatted: Font: Not Bold

Formatted: Font: Not Bold

Formatted: Font: Not Bold

Formatted: Font: Not Bold

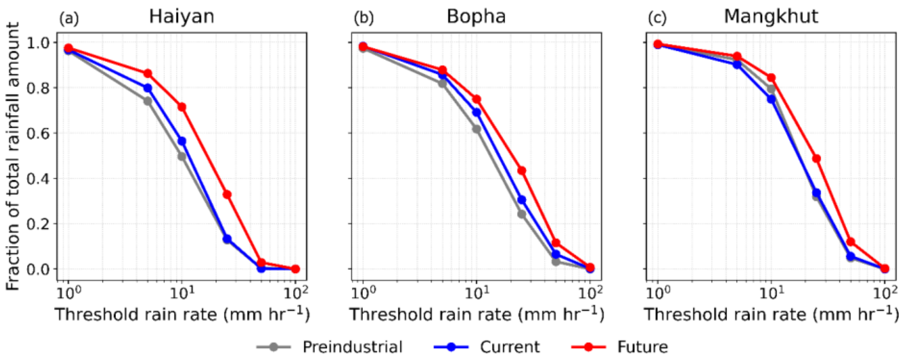

Figure 5. Fraction of total storm rainfall contributed by precipitation exceeding increasing rain-rate thresholds for (a) Haiyan, (b) Bopha, and (c) Mangkhut under preindustrial (gray), current (blue), and future (red) climates. Future simulations shift rainfall contributions toward higher intensities, indicating increasing dominance of extreme precipitation events.

Formatted: Indent: First line: 0"

A recent study by Macalalad et al. (2023) investigated the effects of historical warming on a different TC case, Typhoon Vamco (2020), and showed that the effects of historical warming are counteracted by additional factors such as orography/topography, resulting in comparable precipitation levels between past and present simulations within two river basins in the Philippines. To isolate the topographic effects of TC-associated precipitation, we analysed the TC precipitation rate at the time the simulated TCs reached peak intensity prior to landfall. ~~The percent change in the average rain rate under the future minus current (and current minus pre-industrial) for Typhoon Haiyan is 10% (1%), for Typhoon Bopha is 13% (10%), and for Typhoon Mangkhut is 9% (14%) in the 3kmNoCU experiments. In the 5kmCU experiments, the percent change under the future (pre-industrial) is 17% (1%) for Haiyan, 11% (13%) for Bopha, and 14% (5%) for Mangkhut.~~

The spatial distribution of rainfall rate responses indicates that thermodynamic warming primarily modifies precipitation within the TC inner-core region across all three storms (Figs. 7–9). In both model configurations, increases in rainfall intensity are concentrated within the eyewall and immediately surrounding convective region (approximately within the inner 1.0° radius), where rainfall rates exceeding 20–25 mm h^{-1} become more spatially extensive under future conditions relative to both preindustrial and present-day simulations.

For Typhoon Haiyan (Figure 7), the future simulations show a clear expansion of high rain-rate regions within the eyewall in both dynamical configurations. In the 5 km convection-parameterized (5kmCU) simulations, areas exceeding ~20 mm h^{-1} occupy a substantially larger fraction of the inner-core region compared with the preindustrial case, accompanied by a more azimuthally continuous eyewall structure. The 3 km convection-permitting (3kmNoCU) simulations also show intensified TC inner-core rainfall; however, the response is characterized by localized convective enhancement rather than uniform radial expansion.

The increases in precipitation tend to occur over the TC inner-core regions (Figures 7, 8, and 9, for Typhoon Haiyan, Bopha, and Mangkhut, respectively). The increase in precipitation rates in the inner core regions is more apparent in the 5kmCU runs. In the 3kmNoCU simulations, there are coherent spatial patterns in the future precipitation response characterized by drying in the outer core, resulting in precipitation responses that are stronger over the inner core region in all three TC cases. This drying outer core condition is also present in the 5kmCU future run for Mangkhut. Such drying has also been found by Patricola and Wehner (2018), particularly in the weaker TCs.

Formatted: Indent: First line: 0"

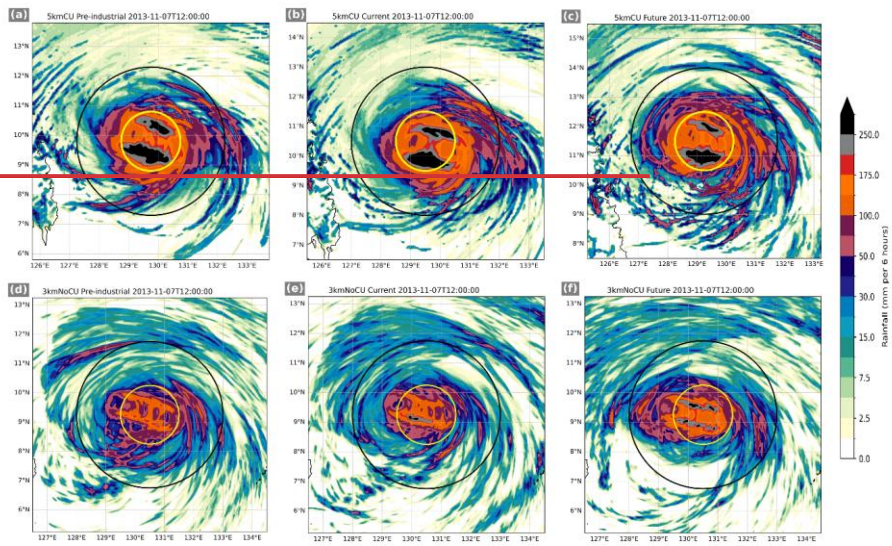

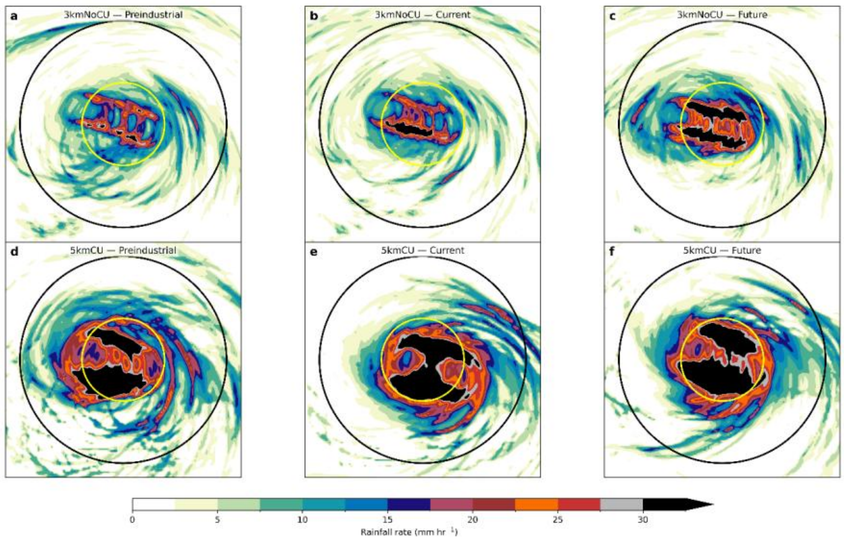

Figure 76. Simulated precipitation rate (mm/hr) at simulated peak intensity for Haiyan on 7 November 2013 12UTC for the 3kmNoCU 5kmCU runs (upper panel) and the 3kmNoCU5kmCU runs (lower panel) under the pre-industrial (left), current (middle), and future climate conditions. The black circle indicates the 2.5° radius from the center, and the yellow circle indicates the 1° radius from the center.

For Typhoon Bopha (Figure 8), the future rainfall response similarly exhibits strengthening of inner-core precipitation, although structural asymmetry remains pronounced. The increase in rainfall intensity is most evident along the primary rainband–eyewall transition region, where rainfall rates above ~15–20 mm h^{-1} expand inward toward the storm center. Compared with Haiyan, outer rainband precipitation shows comparatively weaker enhancement, particularly in the 3kmNoCU simulations.

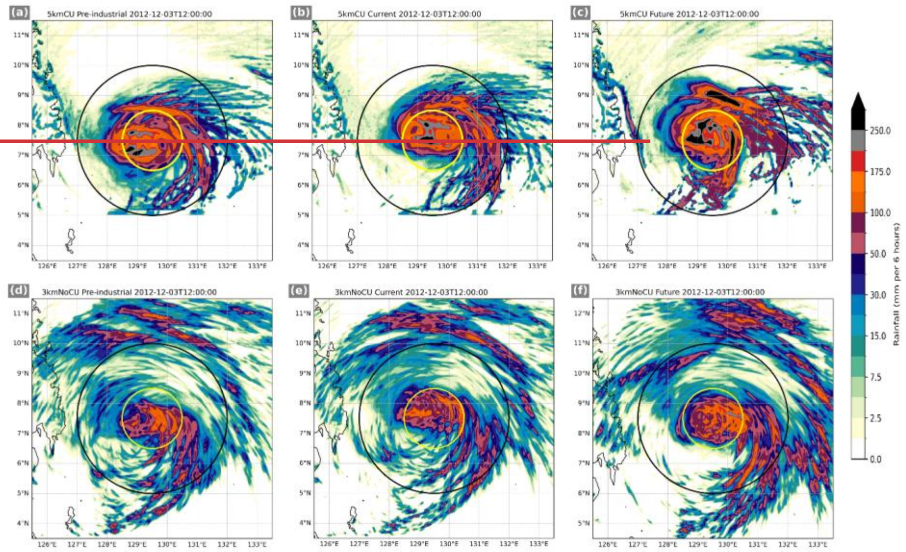

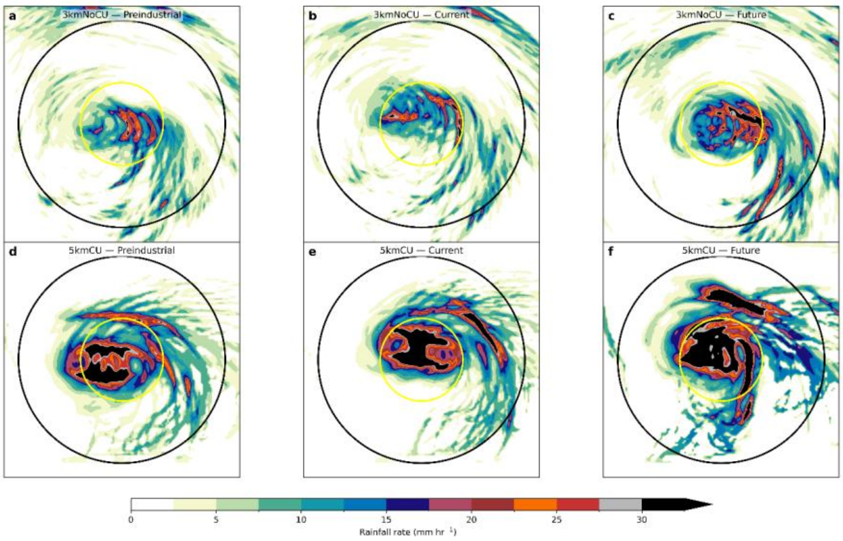

Figure ~~8~~7. Same as Figure ~~7~~6, but for Bopha

Typhoon Mangkhut (Figure 9) displays the strongest structural reorganization among the three TCs. In the 5kmCU simulations, future conditions produce a markedly broader region of intense precipitation surrounding the eyewall, with rainfall rates exceeding 25 mm h^{-1} becoming nearly continuous around the inner-core region. In contrast, precipitation outside the inner-core radius weakens slightly relative to present-day simulations, indicating a redistribution of rainfall toward the TC center. A similar reduction in outer-core precipitation is evident in the 3kmNoCU simulations, suggesting partial drying beyond the eyewall region.

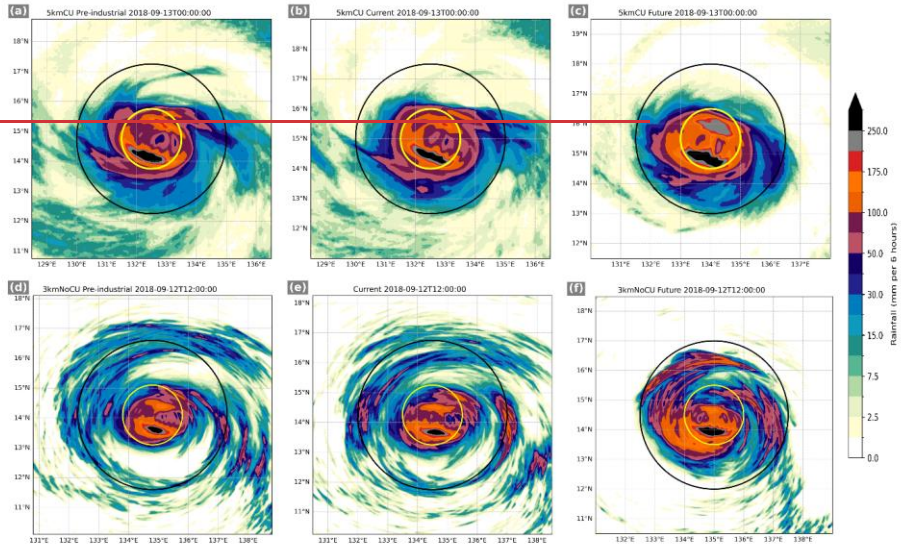

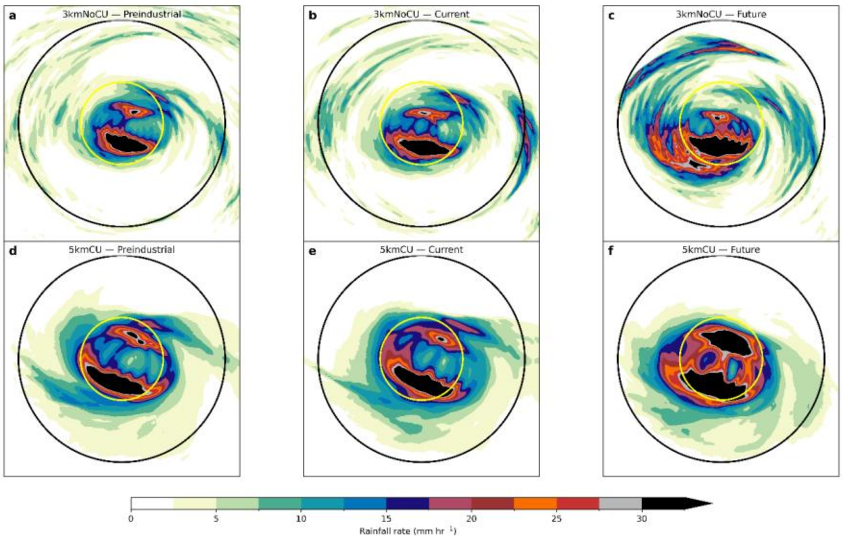

Figure ~~9~~8. Same as Figure ~~7~~6, but for Mangkhut

Across all TCs, increases in precipitation intensity are generally more spatially coherent in the 5kmCU simulations than in the convection-permitting 3kmNoCU runs. The latter exhibit stronger mesoscale variability, with localized convective maxima embedded within otherwise unchanged rainfall envelopes. The apparent reduction or weak response in outer-core precipitation under future conditions implies a radial contraction of rainfall toward the inner core in some cases, consistent with previously reported PGW experiments showing enhanced inner-core precipitation efficiency accompanied by relative outer-core drying (e.g., Patricola and Wehner, 2018), particularly for TCs with weaker large-scale rainband organization.

3.3 Changes in TC rain rate and Clausius-Clapeyron scaling

According to Liu *et al*. (2019), a projected increase in precipitation rate that is more than what is expected according to the CCS relation may be related to the projected increase in TC intensity that is associated with land surface and SST warming. As shown in Figure 109a-c,–under the preindustrial climate, rainfall changes are negative across all TCs despite modest cooling (−0.4 to −0.6 K) and the magnitude of decrease (-5% to -30%) falls below or near the CC scaling (dashed line). In contrast, under future warming (Figure 9e-d), rainfall increases are consistently positive. (~15–30%) for $\Delta SST \approx 2.9$–3.3 K, broadly aligning with the expected ~7% K^{-1} scaling, although some cases (e.g., Mangkhut and Bopha) slightly exceed this thermodynamic benchmark. This indicates that, while the bulk response is largely consistent with CC scaling, there is event-to-event variability that suggests contributions beyond purely thermodynamic control. the largest increases in precipitation tend to occur when only the surface temperatures have been warmed (SFC only). A lower increase is found when atmospheric warming is also included (SFC+PLEV) and RH changes (FULL). In the SFC-only experiments, the future precipitation changes reach more than 17% per degree SST change, which exceeds the CCS relationship. Both the 5kmCU and 3kmNoCU simulations with different initializations (Figure 10b) under the future climate are all within this thermodynamic expectation. The change in rain rate relative to the pre-industrial climate is consistently within the CCS for all typhoons (not shown).

This aligns with the results from Stansfield and Reed (2023), who found that the apparent scaling of TC precipitation in response to SST warming is typically around 6%–9% per K, consistent with the CCS rate, while the climate scaling - which accounts for long-term climate changes - is smaller, around 5% per K. They emphasized that the apparent scaling reflects short-term changes driven by SST alone, while climate scaling incorporates broader atmospheric changes like shifts in wind shear, which reduce the precipitation intensification seen in the SFC-only experiments of Liu et al. (2019).

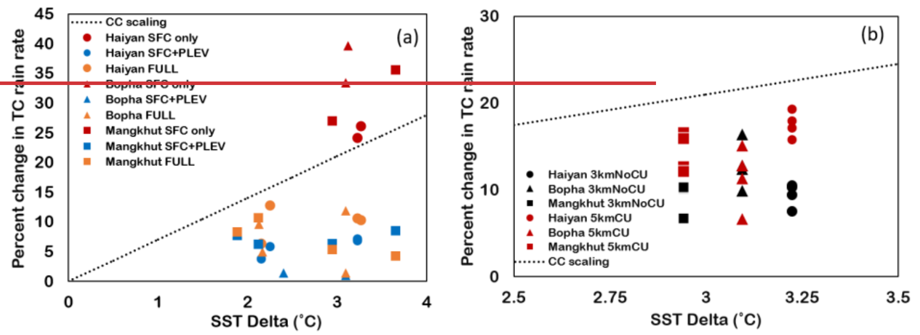

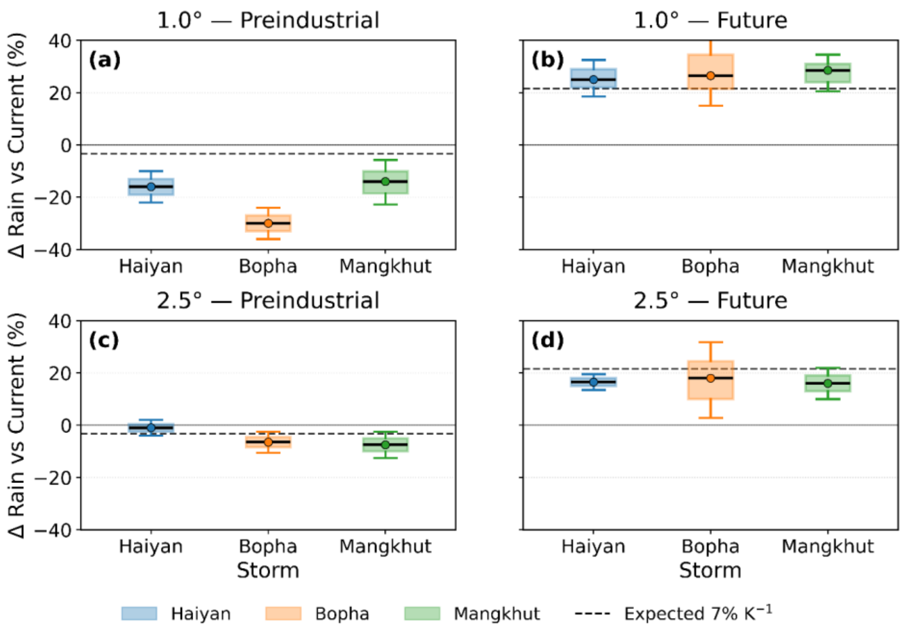

Figure ~~10~~9. ~~Percentage~~ Boxplot of the change in TC ~~inner core~~ rain rates ~~vis-à-vis SST delta.~~ (a) ~~5kmCU~~ within 1.0° radius of the TC for preindustrial vs current climate; (b) within 1.0° radius of the TC for future vs current climate; (c) within 2.5° radius of the TC for preindustrial vs current climate; (b) within 2.5° radius of the TC for future vs current climate~~simulations using different levels of PGW delta and (b) 5kmCU and 3kmNoCU~~ simulations using different initializations. The black dotted lines show the Clausius-Clapeyron scaling.

3.4 Thermodynamic and dynamic decomposition of TC rainfall changes

Figure 10 quantifies the decomposition of the TC rainfall changes into full response (FULL), thermodynamic contribution (TH) and dynamic contribution (DY) for the three TCs under preindustrial and future climate relative to present-day conditions. The decomposition is shown for the different rainfall metrics (azimuthally averaged maximum rainfall rate, rainfall volume, mean rainfall rate). Based on the decomposition, across all three TCs, the most robust signal in the future climate simulations is a positive thermodynamic contribution, ranging typically on the order of 20-30%, irrespective of the rainfall metric. For example, TH is ~+25–30% for Haiyan across Pm, volume, and mean rain, ~+22–27% for Bopha, and ~+20–27% for Mangkhut. This robust signal reflects enhanced moisture availability under warming and aligns with Clausius–Clapeyron expectations. In contrast, the dynamic contribution is smaller and more variable, ranging from about −15% to +10%, and often acts to partially offset the thermodynamic increase. As a result, the net (FULL) response depends strongly on the balance between these two terms. This balance leads to pronounced TC case-to-case differences. Haiyan shows the largest increases, with FULL reaching ~+50% for Pm and ~+25–35% for volume and mean rain; here, TH dominates while DY is weakly negative for Pm (~−10%) and slightly positive (~+5–10%) for both volume and mean rain metrics. In contrast, Bopha exhibits near-zero to weakly negative FULL changes (~−10% to 0%), as a positive TH (~+25%) is nearly cancelled by a negative DY (~−10% to −30%). Mangkhut shows moderate behaviour, with FULL increases of ~+20–25% for Pm and ~+10% for mean rain, but near-zero or slightly negative changes in volume, again due to compensating negative DY (~−5% to −15%). In the preindustrial (PI) experiments, TH is near-zero to slightly negative (≈0 to −3%), while DY largely controls the response: Haiyan shows positive FULL (~+20–25%), Bopha negative (~−15% to −25%), and Mangkhut mixed signals. Overall, these results demonstrate that while thermodynamics sets a fairly uniform positive baseline under warming, dynamical changes determine whether and how strongly that moisture increase translates into rainfall. Our results show that under preindustrial climate, the dynamical contributions are higher than the thermodynamic term, however, under future warming scenarios, the thermodynamic contribution provides the primary positive signal (~20–30%), while dynamics are smaller and often act to offset this increase (≈−10% to −30%).

Formatted: Font: Not Bold

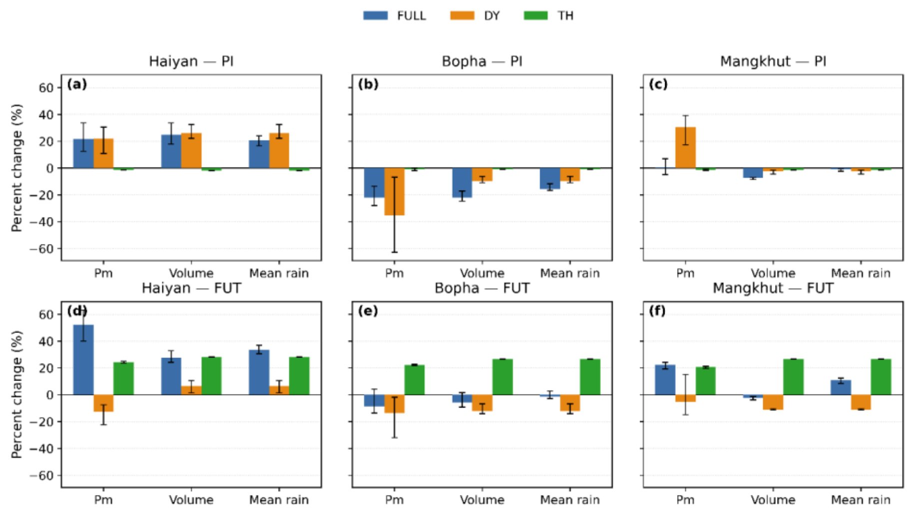

Figure 10. Decomposition of tropical cyclone rainfall changes into full (FULL), thermodynamic (TH), and dynamic (DY) contributions for Haiyan, Bopha, and Mangkhut, shown for preindustrial (PI) and future (FUT) climates relative to present-day conditions. Bars indicate percent changes in azimuthally averaged maximum rainfall rate (Pm), rainfall volume, and mean rainfall rate within 500 km of the storm centre; error bars denote ensemble spread (IQR).

Formatted: Font: Not Bold

3.5 Thermodynamic baseline shift and rainfall sensitivity to intensity change

Figure 11 11 illustrates the relationship between simulated TC intensity and precipitation rate u with separate analysis of the pre-industrial and future climate. The figure indicates that the rainfall–intensity relationship remains positive in both climates, and for peak rainfall metrics such as Pm and P99 the future runs are broadly consistent with the mechanism proposed by Chen et al. (2025), namely that warming enhances the rainfall increase associated with a given intensity increase through greater moisture availability i.e. a 1 ms-1 increase in TC intensity produces a larger rainfall increase. Based on our simulations, the slope is 7.60 % increase in peak rainfall per m s^{-1} and 1.30% increase in extreme rainfall (P99) per m s^{-1} in wind intensity. However, our simulations also reveal pronounced TC case-to-case variability, with some TCs showing substantial dynamic suppression of rainfall despite positive thermodynamic forcing. This suggests that the Chen et al. (2025) relationship holds as a first-order tendency, but its realized magnitude in individual TCs depends strongly on TC structure and dynamics. s TC-specific regressions (Supplementary Figure 1) reveal that warming does not uniformly increase the rainfall response to TC wind intensity changes. When averaged across TCs, the strongest enhancement occurs for azimuthally averaged maximum rainfall rate (Pm), where the future-climate sensitivity reaches 7.6 % per m s−1, compared with −2.4 % per m s−1 in the preindustrial climate. A weaker enhancement is found for P99 rainfall extremes (1.30 vs 1.08 % per m s−1). In contrast, bulk metrics show little or no enhancement, with mean rainfall sensitivities nearly unchanged (2.18 vs 2.29 % per m s−1) and rainfall volume sensitivities lower in the future climate (2.03 vs 4.50 % per m s−1). These results indicate that the warming-enhanced rainfall–intensity relationship proposed by Chen et al. (2025) is most applicable to peak inner-core rainfall rather than total rainfall. ing the 5kmCU and 3kmNoCU experiments for the TC inner core rain rates. The relationship between TC intensity and rain rate in the inner core follows a roughly linear pattern with a regression slope of 0.807 (mm h^{-1}) / (m s^{-1}) (Figure 11a). The 5kmCU and 3kmNoCU under future and pre-industrial climate experiments exhibit a similar rain-rate–intensity relationship in the TC inner core, with the regression slope of 0.38 (mm h^{-1})/ (m s^{-1}) (Figure 11b). We found that the rain rate in the TC inner core is positively correlated with TC intensity. Specifically, a 1 m s^{-1} increase in TC intensity leads to approximately a 1.17 mm h^{-1} increase in TC rain rate in the 5kmCU simulations and an average of 0.66 mm h^{-1} increase in the 3kmNoCU simulations. Given the sensitivity of TC intensity to SST and the dependency of rain rate on TC intensity, we explored the sensitivity of TC precipitation to SST. Our findings indicate that the TC inner-core rain rate of the three TC cases (for both 3kmNoCU and 5kmCU runs) will increase by approximately 6% per 1 K increase in SST in the future. This increase can be understood through the combined effects of TC intensity sensitivity to SST and CCS. However, larger increases (up to 33% per 1K increase in SST) can be found in the 5kmCU SFC-only experiments, which may be due to the changes in thermodynamics and shifts in TC trajectory (Delfino et al., 2023). The rest of the simulations under the 5kmCU SFC+PLEV and FULL and 3kmNoCU experiments show no significant changes in track.

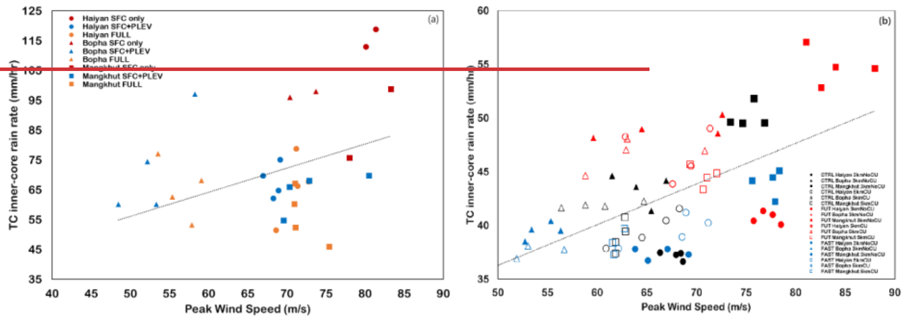

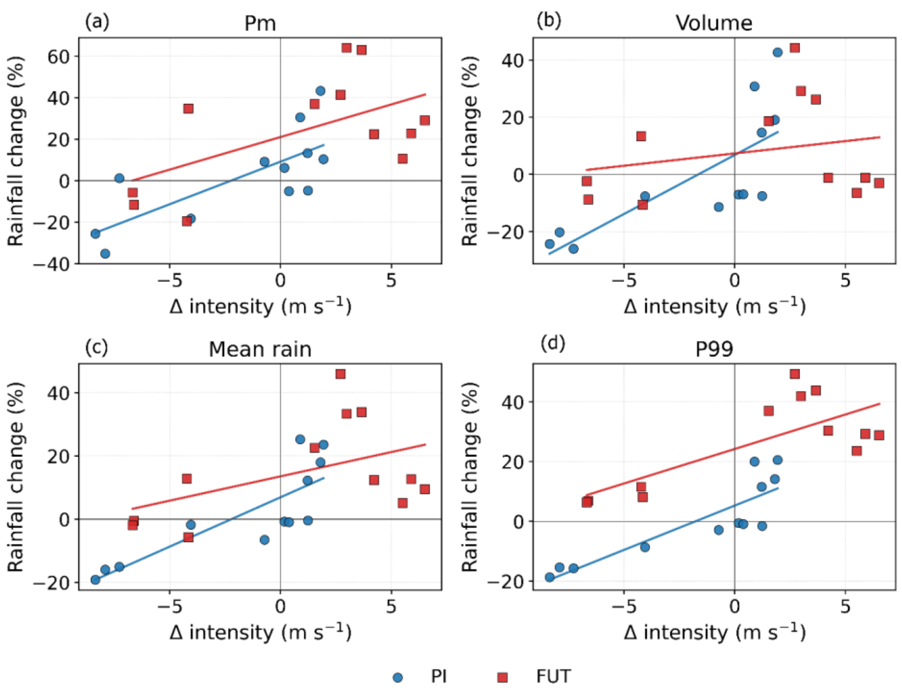

Figure ~~11~~11. Relationship between changes in tropical cyclone intensity (Δ intensity, m s^{-1}) and rainfall response for preindustrial (PI; blue) and future (FUT; red) simulations. Panels show percent changes in (a) azimuthally averaged maximum rainfall rate (Pm), (b) rainfall volume, (c) mean rainfall rate, and (d) extreme rainfall (P99). Solid lines indicate linear fits for each climate state, highlighting a stronger and more consistent positive scaling between intensity and rainfall under future warming compared to preindustrial conditions.~~Dependence of TC inner-core rain rate on TC intensity. (a) 5kmCU simulations~~

~~**using different levels of PGW delta and (b) 5kmCU and 3kmNoCU simulations using different initializations.**~~

3.4 Potential mechanisms driving TC-associated precipitation changes

Figure ~~12~~ 12 shows the ~~vertical profiles of the averaged~~ radius-height composites of simulated reflectivity (dBZ) ~~over a~~within the 2.5° radius in the forward direction of the ~~storm~~ TCs at peak intensity for the 3kmNoCU simulations, the 5kmCU simulations (not shown) reveal similar results. The vertical expansion of the eyewall, the inner region of a TC characterized by intense convection and the strongest winds surrounding the eye, is consistent with the vertical cross-sections of composite azimuthally averaged winds reported by Delfino et al. (2023). As indicated by the increased reflectivity in Figure 12, these changes provide insight into the evolving structure of TCs under the different climate conditions simulated in this study. Although the compositing was performed at the peak intensity of the storms, the results reveal substantial enhancements in reflectivity throughout the vertical extent and within a 2.5° radius in the forward sector of the TC circulation. The largest positive reflectivity anomalies in the future-minus-current simulations are concentrated near the eyewall and inner-core region, particularly through the mid- to upper troposphere, indicating deeper convection and stronger precipitation-producing clouds. In contrast, the pre-industrial-minus-current simulations generally show weaker reflectivity in the lower- to midlevel inner core, suggesting that present-day climates already favor stronger and more vertically developed precipitation structures than pre-industrial conditions.

This enhanced reflectivity implies a greater amount of precipitation within the TC inner core, with important consequences for storm dynamics. The explanation for the vertical expansion of the eyewall likely lies in the interaction between thermodynamic and dynamic atmospheric processes. Earlier scaling analyses in this study showed that projected rainfall increases cannot be explained solely by thermodynamic moisture increases associated with Clausius–Clapeyron scaling. If thermodynamic forcing alone dominated, changes would be more spatially uniform. Instead, Figure 12 shows that the strongest increases are concentrated in dynamically active regions such as the eyewall slope and inner-core convective towers, indicating that structural changes in storm circulation also play a critical role. ~~The compositing is done at peak intensity and at height levels between 0 and 18 km. This shows that there are substantial increases in simulated reflectivity (which could translate into precipitation) over the vertical extent, particularly within the TC's primary circulation. Overall, an increase in precipitation corresponds to an increase in latent heating (shown in Figure 13), which results in a deeper core convection of the TC cases in the future, as seen in the upward extension of the eyewall / vertical expansion of the eyewall.~~

Formatted: Space After: 0 pt

~~The vertical expansion of the eyewall, the inner region of TC with intense convection and strongest winds surrounding the eye of the storm, is consistent with what is found in the vertical cross-section of the composite of azimuthally averaged winds (Delfino et al., 2023), and, as indicated by the increased reflectivity observed in Figure 12, provides insights into the evolving structure of TCs under the different climate conditions simulated in the study. While the compositing is performed at the peak intensity of the TCs, the results reveal substantial~~

~~enhancements in reflectivity throughout the vertical extent within a 2.5° radius around the TC's forward direction. This enhanced reflectivity suggests a greater amount of precipitation within the TC's inner core, which has implications for its overall dynamics. The explanation for the vertical expansion of the eyewall lies in the interactions between different atmospheric processes.~~ As TC intensity increases, precipitation rates within the storm also tend to increase (Alvey et al., 2015), reflecting and reinforcing internal dynamical processes critical to intensification. While environmental conditions such as warm sea surface temperatures, low vertical wind shear, and high low-level moisture are known to support TC development (DeMaria et al., 2005; Kaplan et al., 2010, 2015), they do not fully account for changes in TC intensity (Hendricks et al., 2010). This has led to a growing focus on internal TC processes, particularly precipitation and convection, as key drivers of TC intensification. Latent heat release from enhanced precipitation warms the TC core and contributes to further pressure falls, strengthening the cyclone (Rotunno & Emanuel, 1987; Pendergrass, 2014; Yamada, 2017). Observational studies using TRMM and passive microwave data have shown that more intense TCs are typically associated with broader and more symmetric precipitation coverage, especially in the inner core (Alvey et al., 2015). Stratiform and moderate-to-deep convective precipitation are particularly linked to rapid intensification (Tao & Jiang, 2015), suggesting that increasing precipitation is not just a result of intensification, but a contributor to it. Ruan and Wu (2018) also found that as TCs intensify, they exhibit increased precipitation and colder high cloud tops, and that widespread very deep convective clouds (IR BT < 208 K) are strong predictors of future intensity change, particularly rapid intensification (Tierra and Bagtasa 2021).

Formatted: Font: (Default) Times New Roman, 10 pt

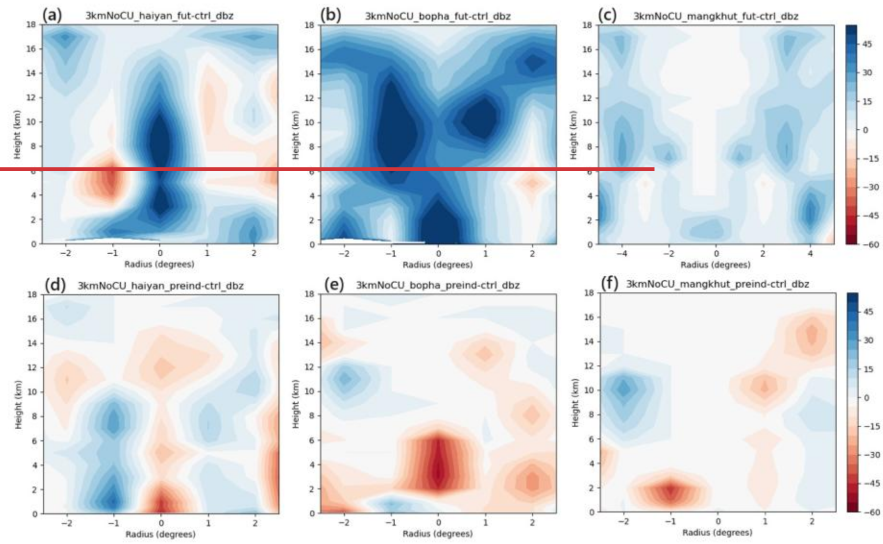

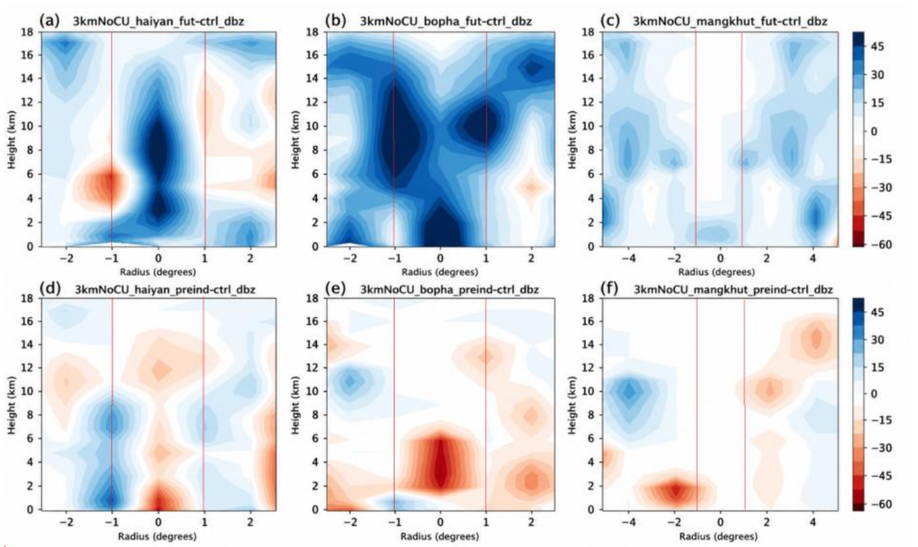

Formatted: Not Highlight

Figure ~~12~~12. Radius (in degrees) – height (in km) cross sections of simulated differences in reflectivity (dBZ) from future minus current (top panels, a-c) and pre-industrial minus current (bottom panel, d-f) from the 3kmNoCU experiments. All reflectivity fields are at peak intensity while precipitation rates are shown within a 2.5° x 2.5° ~~grid~~ from the center at peak intensity for Typhoon Haiyan (a and d panels), Bopha (b and e panels), and Mangkhut (c and f panels) with the red vertical lines delineating 1° radius from the center.

Vertical motion (omega) was investigated to better understand the detailed processes governing TC-associated precipitation intensification under different climate conditions (Figure 13). Our analysis revealed significant regions of enhanced upward motion near the eyewall and along spiral rainbands of Typhoons Haiyan, Bopha, and Mangkhut, primarily within a 1° and 2.5° radius from the TC center. These regions are critical for intense convective activity and high precipitation rates because vigorous updrafts promote condensation and latent heat release. Comparisons between future and current climate simulations show stronger and deeper ascent around the TC core region, consistent with the enhanced reflectivity shown in Figure 13a-c. The strongest omega anomalies are concentrated in the same regions where reflectivity increases are maximized, reinforcing the interpretation that dynamic strengthening of convection contributes substantially to future rainfall intensification.

Formatted: Font: Not Bold

Similarly, the pre-industrial-minus-current simulations reveal weaker and shallower ascent relative to the present climate, especially in the inner-core region. This corresponds closely with the weaker reflectivity anomalies in Figure 13 and suggests that the present climate already supports stronger moisture convergence and more vigorous convection than the pre-industrial environment. Thus, the transition from pre-industrial to current to future climates indicates a progressive strengthening of the vertical overturning circulation and precipitation efficiency of intense TCs.

In our earlier study, Delfino et al. (2023) noted shifts in the vertical profiles of these TC cases that potentially led to intensified rainfall. Additionally, Shi et al. (2024) showed that TCs may evolve not simply through stronger localized updrafts, but through the expansion of deep convective cores while suppressing shallow cumulus and congestus clouds. This structural reorganization implies that, although localized hourly rainfall may scale close to Clausius–Clapeyron expectations, precipitation accumulation over broader storm areas could increase by as much as 18% per degree of warming. Taken together, Figures 12 and 13 show that projected TC rainfall increases arise from both thermodynamic and dynamic mechanisms. Increased moisture availability provides the thermodynamic basis for heavier precipitation, while stronger eyewall ascent, deeper convective towers, and broader precipitation cores determine where the largest rainfall intensification occurs. Therefore, the simulated precipitation response is best interpreted as a coupled thermodynamic–dynamic scaling process rather than a purely moisture-driven one.Vertical motion (omega) was investigated to understand the detailed processes of TC-associated precipitation intensification in different climate conditions (Figure 13). Our analysis revealed significant regions of strong ascending motion, characterized by increased omega, near the eyewall and along spiral rainbands of Typhoons Haiyan, Bopha, and Mangkhut, primarily within a 250-km radius from the TC center. These regions are crucial for intense convective activity and high precipitation rates due to vigorous updrafts and condensation processes. Comparisons between future and current climate simulations highlighted larger differences in omega around the TC core region, indicating a potential increase in vertical motion and precipitation rates under projected future climates. Similarly, significant differences were noted between current and past climate scenarios, suggesting consistent changes in vertical motion patterns over time. Our findings regarding the differences in omega between current and future climate simulations suggest a projected increase in vertical motion and moisture convergence, which will likely lead to stronger precipitation events. In our earlier study (Delfino et al., 2023), we note that there are some changes or shifts in the vertical profiles of the TC cases that potentially led to the further intensification of rainfall associated with these TCs. Additionally, Shi et al. (2024) noted that instead of TCs solely intensifying due to strengthened updrafts, TCs are projected to evolve through the expansion of deep convective cores while suppressing shallow cumulus and congestus clouds. This structural change means that, while localized hourly rainfall may follow the CCS, precipitation accumulation over larger areas could surge by as much as 18% per degree of warming.

Understanding these dynamics is essential for predicting how TCs may evolve under different climate scenarios, particularly in terms of intensity and precipitation distribution. Overall, the study underscores the sensitivity of TC dynamics to changes in vertical motion and provides insights into the complex interactions shaping TC-associated precipitation, contributing to advancing our understanding of TC characteristics in a changing climate.

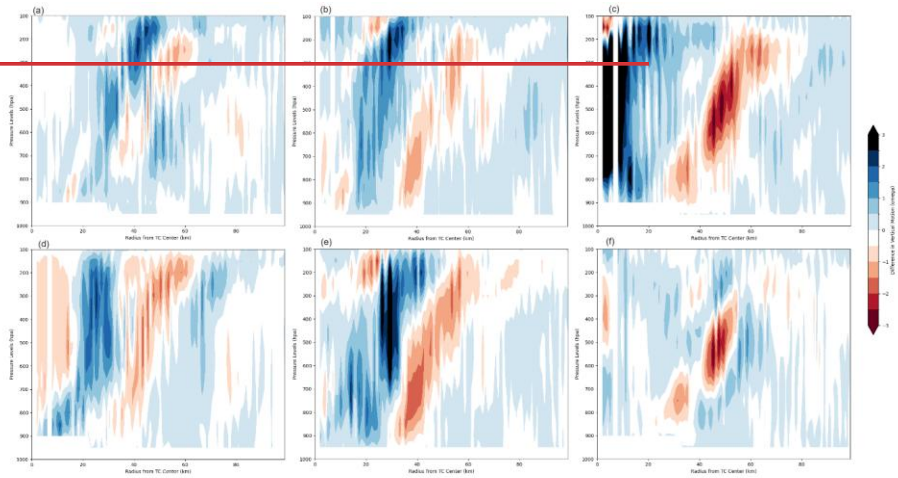

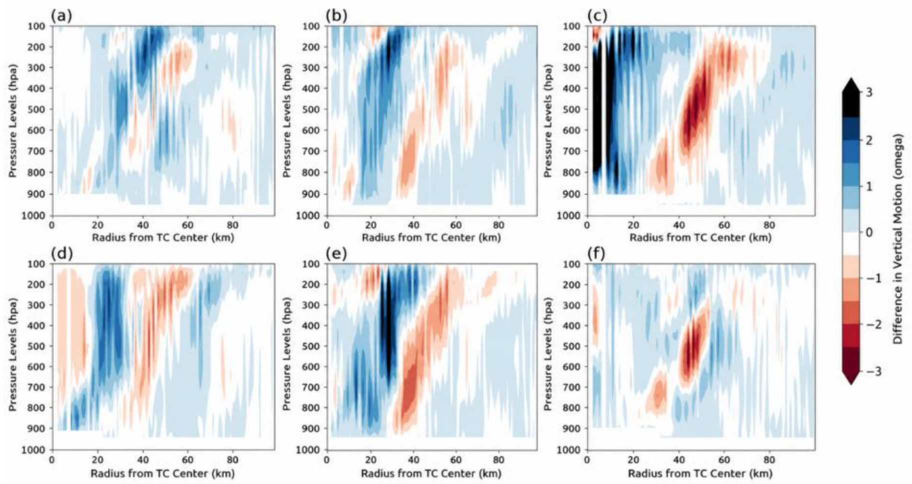

Figure 1313. Simulated difference in vertical velocity, Omega (hPa s−1) at several levels (1000-100hPa) within 250 km radius from the TC center for the 3kmNoCU experiments difference between future and current climate (top, a-c), and difference between current and past climate (bottom, d-f) for Typhoons Haiyan (left), Bopha (center) and Mangkhut (right).

Formatted: Not Highlight

Formatted: Not Highlight

Formatted: Not Highlight

4. Summary and conclusions

This study has investigated the changes in tropical cyclone (TC)-associated precipitation in the Philippines under past (pre-industrial) and future climate scenarios, using a hierarchy of convection-permitting simulations. Importantly, this is the first time that such extreme typhoons have been systematically simulated and compared using both convection-permitting and parameterised convection models. Some of the results show a sensitivity to the treatment of convection, while other experiments are relatively insensitive. Overall, the main findings are robust and largely insensitive to this model formulation choice. In alignment with the expectations from Clausius–Clapeyron scaling (CCS) for TCs, the future climate simulations project a robust increase in TC precipitation. Deviations from the expected CCS scaling are attributed to factors such as increased TC intensity, also driven by atmospheric warming.

Under past climate conditions, TC precipitation in the Philippines would have been generally less than that of current climate conditions, with an average change (current - past) in TC inner-core precipitation rates of 6% and 8% for the 5kmCU and 3kmNoCU experiments, respectively. The observed changes between the past and current climate align with expectations from CCS, indicating that the atmosphere holds approximately 7% more water vapor per degree Celsius increase in surface temperature. Conversely, under future climate scenarios, the FULL simulations conducted under the SSP5-8.5 scenario indicate a robust rise - by approximately 6% per 1 K increase in SST in the mean precipitation rates for specific intense TCs, such as Haiyan, Bopha, and Mangkhut, in both the 5kmCU and 3kmNoCU experiments, consistent with CCS expectations.

Based on our simulations, the dynamic process is larger under preindustrial simulations, and the thermodynamic processes dominate TC rainfall changes under warming. Decomposition analysis shows a robust positive thermodynamic contribution (~20–30%) across all TCs and rainfall metrics, while dynamical contributions are smaller and often negative (~−10% to −30%), partially offsetting the thermodynamic increase. This leads to substantial TC cases variability: Haiyan shows strong net increases, Bopha exhibits near-cancellation between thermodynamic and dynamical effects, and Mangkhut displays moderate increases with partial dynamic suppression. These results suggest that dynamical dominance indicate that moisture increases set the baseline rainfall response, with dynamics modulating its magnitude and spatial distribution.

Future warming also produces a systematic intensification of rainfall extremes. The upper tail of the rainfall distribution (P99) increases disproportionately, with enhancements exceeding 30–40% in some cases. Additionally, the fractional contribution of heavy rainfall increases, indicating a shift toward more intense, short-duration precipitation events concentrated in the TC inner core. Spatial analyses show that rainfall increases are primarily concentrated within the inner-core region, with some cases exhibiting outer-core weakening or radial contraction of rainfall, particularly for structurally organized storms like Mangkhut. This suggests increased precipitation efficiency near the eyewall under warming.

The relationship between TC intensity and rainfall remains positive in both future and pre-industrial climates. However, warming preferentially enhances the sensitivity of peak rainfall (Pm) to intensity (~7.6% per m s^{-1}), while bulk metrics (mean rainfall and volume) show little or no enhancement. This indicates that intensity–rainfall scaling strengthens mainly for extreme inner-core precipitation rather than total storm rainfall.However, notable deviations from CCS arise in simulations where only the land and sea surface temperatures are increased (e.g., 5kmCU SFC-only), with precipitation increases reaching up to 13% per 1 K SST increase. This suggests that additional dynamical processes, such as TC track changes or structural modifications, amplify precipitation beyond thermodynamic expectations. Frequency distributions of rainfall further confirmed an intensification of heavy precipitation events in a warming climate. Future scenarios displayed a consistent shift toward higher 6-hourly rainfall rates, particularly in the right tail (extreme values).

Notably, the results reveal an asymmetry in the response of TC precipitation between past cooling and future warming. Specifically, under future warming, feedback appears to amplify precipitation (consistent with a positive feedback mechanism), while in the pre-industrial simulations, these feedbacks act in the opposite direction, dampening TC intensity and precipitation.

Spatial analysis of accumulated precipitation revealed that rainfall over land also increased from preindustrial to current climates, and will increase even more from current to future scenarios, particularly for Typhoons Haiyan and Bopha. Mangkhut, however, showed a relatively minimal response primarily in the land-only rainfall under future conditions, primarily due to the slight northward shift in tracks. Overall, the total accumulated rainfall associated with the three TCs, within a 2.5° radius, is expected to increase by up to 25% in the future.

The analysis of simulated reflectivity profiles of the three TC cases reveals further insights into future climate conditions, with increases in both outward and vertical extent of maximum reflectivity indicating more intense and widespread precipitation. This is attributed to enhanced latent heating, which drives stronger updrafts and contributes to a deeper TC core. Mechanistically, the deeper cores lead to intensified updrafts that enhance the lift of moist air, promoting additional adiabatic warming within the TC and further enhancing TC-associated precipitation. This chain of causation aligns with previous studies (e.g., Yamada et al., 2017) that emphasize the role of latent heating in TC dynamics.

Our findings provide critical insightscrucial insights into how variations in TC intensity and structure influence the scaling relationship between SST and TC-associated precipitation in the Philippines. The heightened intensity of simulated TCs under future climate conditions contributes to increased TC-associated precipitation rates within the inner core, diverging from expected CCS behavior. This supports the notion of the CCS, emphasizing the interplay between atmospheric moistening, TC dynamics, and evolving TC structures.

We recommend that future studies focus on (1) the climatological trends in TC precipitation i.e. effects of climate change and natural climate variabilities on TC precipitation needs to be done with simulations that are able to simulate TCs with good fidelity; (2) the specific impacts of changing TC tracks ~~, the~~and the role of atmospheric moisture distribution, and (3) the influence of varying SST patterns and magnitude on TC-associated precipitation in the Philippines. Additionally, further research should investigate the potential effects of land-use changes and urbanization on TC rainfall patterns to provide a more comprehensive understanding of the local impacts of climate change on TCs.

AUTHOR DECLARATIONS

Funding Information

Rafaela Jane Delfino was supported by a scholarship under the Philippine Commission for Higher Education and British Council under the Joint Development of Niche Programme through Philippines-UK Linkages (JDNP) Dual PhD Program. Kevin Hodges and Pier Luigi Vidale is funded by the RCUK through the Natural Environment Research Council (Grant number: NE/W009587/1). This research used resources of the JASMIN data analysis facility, the UK's collaborative data analysis environment (https://www.jasmin.ac.uk). For the additional analysis made in this paper, Gerry Bagtasa and Rafaela Jane Delfino were supported by the University of the Philippines Diliman Natural Sciences Research Institute (NSRI) under the project entitled "*Investigating the effects of past and future changes in climate on a collection of Philippine Super Typhoons and their flooding potential from the last 10 years (2012 – 2022) using a convection-permitting regional climate model" (ESM-24-1-01).* We thank the two anonymous reviewers for the valuable comments and suggestions.

Author Contributions

RJD conceptualized and designed the experiments. Data preparation, simulations and analysis were performed by RJD, with guidance and support particularly in the interpretation of results by GB, PLV and KH. The first draft of the manuscript was written by RJD and all authors contributed to all versions of the manuscript. All authors read and approved the final manuscript.

Conflicts of Interest

I declare that the authors have no competing interests as defined by Copernicus Publications, or other interests that might be perceived to influence the results and/or discussion reported in this paper

Ethics approval/declarations (include appropriate approvals or waivers)

Not applicable

Consent to participate (include appropriate statements)

Not applicable

Consent for publication (include appropriate statements)

Not applicable

Data and Code Availability

Simulation data are stored at the JASMIN data storage facility and are available upon request from the corresponding author. Code for the WRF model is available at http://www.www2.mmm.ucar.edu/wrf/users/downloads.html. WPS geographical input data are available from https://www.www2.mmm.ucar.edu/wrf/users/download/get_sources_wps_geog.html#mandatory.TRACK is available from https://gitlab.act.reading.ac.uk/track/track/-/releases . CF-python and CF-plot were used in the analysis and visualization, and installation packages are available from https://www.ncas-cms.github.io/cf-python/. The CEDA-JASMIN facility was used in the analysis and storage of data.

The analysis codes and simulation data are available upon request to the corresponding author. ~~The CEDA-JASMIN facility was used in the analysis and storage of data.~~

References

Adachi, S. A., & Tomita, H. (2020). Methodology of the constraint condition in dynamical downscaling for regional climate evaluation: A review. Journal of Geophysical Research: Atmospheres, 125, e2019JD032166. https://doi.org/10.1029/2019JD032166

Allen, M. R., & Ingram, W. J. (2002). Constraints on future changes in climate and the hydrologic cycle. Nature, 419(6903), 224–232. https://doi.org/10.1038/nature01092

Alvey, G. R., III, Zawislak, J., & Zipser, E. J. (2015). Precipitation properties observed during tropical cyclone intensity change. Monthly Weather Review, 143(11), 4476–4492. https://doi.org/10.1175/MWR-D-15-0065.1

Bagtasa, G. (2017). Contribution of tropical cyclones to precipitation in the Philippines. Journal of Climate, 30, 3621–3633. https://doi.org/10.1175/JCLI-D-16-0150.1

Bagtasa, G. (2021). Analog forecasting of tropical cyclone precipitation in the Philippines. Weather and Climate Extremes, 32, 100323. https://doi.org/10.1016/j.wace.2021.100323

Bagtasa, G. (2022). Variability of tropical cyclone precipitation volume in the Philippines. International Journal of Climatology, 42, 7573–7588. https://doi.org/10.1002/joc.7573

Bhatia, K. T., Vecchi, G. A., Murakami, H., Underwood, S., & Kossin, J. P. (2018). Projected response of tropical cyclone intensity and intensification in a global climate model. Journal of Climate, 31, 8281–8303. https://doi.org/10.1175/JCLI-D-17-0898.1

Formatted: Indent: Hanging: 0.25"

Formatted: Indent: Left: 0", Hanging: 0.25"

Cha, E. J., Knutson, T. R., Lee, T. C., Ying, M., & Nakaegawa, T. (2020). Third assessment on impacts of climate change on tropical cyclones in the Typhoon Committee Region–Part II: Future projections. Tropical Cyclone Research and Review, 9(2), 75–86. https://doi.org/10.1016/j.tcrr.2020.04.005

Chen, J., Toumi, R., Zhang, L., Lu, M., Xi, D., & Shi, X. (2025). Radial rainfall pattern changes of intense over-ocean tropical cyclones under global warming: Insights from an MRI HighRes CMIP6 simulation. Geophysical Research Letters, 52(9), e2025GL116146.

Formatted: Indent: Left: 0", Hanging: 0.25"

Cinco, T. A., de Guzman, R. G., Ortiz, A. M. D., Delfino, R. J. P., Lasco, R. D., Hilario, F. D., & Ares, E. D. (2016). Observed trends and impacts of tropical cyclones in the Philippines. International Journal of Climatology, 36(14), 4638–4650. https://doi.org/10.1002/joc.4659

Cruz, F. T., Tacan, F. P., Uy, N. T. P., & Santillan, J. R. (2020). Topographical effects on precipitation distribution during typhoons in the Philippines. Natural Hazards, 103(1), 1003–1020. https://doi.org/10.1007/s11069-020-04057-0

da Silva, N. A., & Haerter, J. O. (2025). Super-Clausius–Clapeyron scaling of extreme precipitation explained by shift from stratiform to convective rain type. Nature Geoscience, 18, 382–388. https://doi.org/10.1038/s41561-025-01686-4

DeMaria, M., Mainelli, M., Shay, L. K., Knaff, J. A., & Kaplan, J. (2005). Further improvement to the Statistical Hurricane Intensity Prediction Scheme (SHIPS). Weather and Forecasting, 20(4), 531–543. https://doi.org/10.1175/WAF862.1

Delfino, R. J. P., Bagtasa, G., Hodges, K., & Vidale, P. L. V. (2022). Sensitivity of simulating Typhoon Haiyan (2013) using WRF: The role of cumulus convection, surface flux parameterizations, spectral nudging and initial and boundary conditions. Natural Hazards and Earth System Sciences, 22, 3285–3307. https://doi.org/10.5194/nhess-22-3285-2022

Delfino, R. J. P., Hodges, K., Vidale, P. L. V., & Bagtasa, G. (2024). Sensitivity of Philippine historically damaging tropical cyclone events to surface and atmospheric temperature forcings. Regional Studies in Marine Science, 69, 103595. https://doi.org/10.1016/j.rsma.2024.103595

Delfino, R. J. P., Vidale, P. L. V., Bagtasa, G., & Hodges, K. (2023). Response of damaging tropical cyclone events in the Philippines to climate forcings from selected CMIP6 models using the pseudo global warming technique. Climate Dynamics, 61, 6743–6765. https://doi.org/10.1007/s00382-023-06742-6

Emanuel, K. (2005). Increasing destructiveness of tropical cyclones over the past 30 years. Nature, 436(7051), 686–688. https://doi.org/10.1038/nature03906

Emanuel, K. A. (1986). An air–sea interaction theory for tropical cyclones. Part I: Steady-state maintenance. Journal of the Atmospheric Sciences, 43, 585–604. https://doi.org/10.1175/1520-0469(1986)043<0585:AAITFT>2.0.CO;2

Emanuel, K. A. (1987). The dependence of hurricane intensity on climate. Nature, 326(6112), 483–485. https://doi.org/10.1038/326483a0

Eyring, V., Bony, S., Meehl, G. A., et al. (2016). Overview of the Coupled Model Intercomparison Project Phase 6 (CMIP6) experimental design and organization. Geoscientific Model Development, 9, 1937–1958. https://doi.org/10.5194/gmd-9-1937-2016

Held, I. M., & Soden, B. J. (2006). Robust responses of the hydrological cycle to global warming. Journal of Climate, 19(21), 5686–5699. https://doi.org/10.1175/JCLI3990.1

Huprikar, A. S., Stansfield, A. M., & Reed, K. A. (2023). A storyline analysis of Hurricane Irma's precipitation under various levels of climate warming. Environmental Research Letters, 19, 014004. https://doi.org/10.1088/1748-9326/ad0e67

Intergovernmental Panel on Climate Change. (2021). Climate change 2021: The physical science basis. Cambridge University Press. https://doi.org/10.1017/9781009157896

Knutson, T. R., et al. (2010). Tropical cyclones and climate change. Nature Geoscience, 3(3), 157–163. https://doi.org/10.1038/ngeo779

Knutson, T. R., et al. (2015). Global projections of intense tropical cyclone activity for the late twenty-first century from dynamical downscaling of CMIP5/RCP4.5 scenarios. Journal of Climate, 28, 7203–7224. https://doi.org/10.1175/JCLI-D-15-0129.1

Kossin, J. P., Emanuel, K. A., & Vecchi, G. A. (2014). The poleward migration of the location of tropical cyclone maximum intensity. Nature, 509, 349–352. https://doi.org/10.1038/nature13278

Lenderink, G., Barbero, R., Loriaux, J. M., & Fowler, H. J. (2017). Super-Clausius–Clapeyron scaling of extreme hourly convective precipitation and its relation to large-scale atmospheric conditions. Journal of Climate, 30, 6037–6052. https://doi.org/10.1175/JCLI-D-16-0808.1

Liu, M., Vecchi, G. A., Smith, J. A., & Murakami, H. (2019). Causes of large projected increases in hurricane precipitation rates with global warming. npj Climate and Atmospheric Science, 2, 38. https://doi.org/10.1038/s41612-019-0095-3

Montgomery, M. T., Persing, J., & Smith, R. K. (2015). Putting to rest WISHE-ful misconceptions for tropical cyclone intensification. Journal of Advances in Modeling Earth Systems, 7(1), 92–109. https://doi.org/10.1002/2014MS000362

O'Gorman, P. A. (2015). Precipitation extremes under climate change. Current Climate Change Reports, 1, 49–59. https://doi.org/10.1007/s40641-015-0009-3

Pendergrass, A. G., & Hartmann, D. L. (2014). Two modes of change of the distribution of rain. Journal of Climate, 27, 8357–8371. https://doi.org/10.1175/JCLI-D-14-00182.1

Rotunno, R., & Emanuel, K. A. (1987). An air–sea interaction theory for tropical cyclones. Part II: Evolutionary study using a nonhydrostatic axisymmetric numerical model. Journal of the Atmospheric Sciences, 44, 542–561. https://doi.org/10.1175/1520-0469(1987)044<0542:AAITFT>2.0.CO;2

Shi, X., Liu, Y., Chen, J., et al. (2024). Escalating tropical cyclone precipitation extremes and landslide hazards in South China under global warming. npj Climate and Atmospheric Science, 7, 107. https://doi.org/10.1038/s41612-024-00654-w

Stansfield, A. M., & Reed, K. A. (2023). Global tropical cyclone precipitation scaling with sea surface temperature. npj Climate and Atmospheric Science, 6, 60. https://doi.org/10.1038/s41612-023-00391-6

Tao, C., & Jiang, H. (2015). Distributions of shallow to very deep precipitation-convection in rapidly intensifying tropical cyclones. Journal of Climate, 28(22), 8791–8824. https://doi.org/10.1175/JCLI-D-14-00448.1

Vecchi, G. A., et al. (2019). Tropical cyclone sensitivities to CO_2 doubling: Roles of atmospheric resolution, synoptic variability and background climate changes. Climate Dynamics. https://doi.org/10.1007/s00382-019-04913-y

Xi, D., Wang, S., & Lin, N. (2023). Analyzing relationships between tropical cyclone intensity and rain rate over the ocean using numerical simulations. Journal of Climate, 36(1), 81–91. https://doi.org/10.1175/JCLI-D-22-0141.1

Yamada, Y., Satoh, M., Sugi, M., Kodama, C., Noda, A. T., Nakano, M., & Nasuno, T. (2017). Response of tropical cyclone activity and structure to global warming in a high-resolution global nonhydrostatic model. Journal of Climate, 30, 9703–9724. https://doi.org/10.1175/JCLI-D-17-0068.1

Yang, Y., & Toumi, R. (2025). Large dynamic contributions to tropical cyclone precipitation with increasing sea surface temperature. Environmental Research Letters, 20(7), 074013.

Yoshida, K., Sugi, M., Mizuta, R., Murakami, H., & Ishii, M. (2017). Future changes in tropical cyclone activity in high-resolution large-ensemble simulations. Geophysical Research Letters, 44, 9910–9917. https://doi.org/10.1002/2017GL075058

Allen, M. R., & Ingram, W. J. (2002). Constraints on future changes in climate and the hydrologic cycle. *Nature*, *419*(6903), 224-232.

Alvey, G. R. III, Zawislak, J., & Zipser, E. (2015). Precipitation properties observed during tropical cyclone intensity change. Monthly Weather Review, 143(11), 4476–4492. https://doi.org/10.1175/MWR-D-15-0065.1

Bagtasa, G. (2017): Contribution of Tropical Cyclones to Precipitation in the Philippines. Journal of Climate. Vol 30. pp. 3621-3633. http://dx.doi.org/10.1175/JCLI-D-16-0150.1

Bagtasa, G. (2021): Analog forecasting of tropical cyclone precipitation in the Philippines,J. Weather and Climate Extremes,32, https://doi.org/10.1016/j.wace.2021.100323

Bagtasa, G. (2022). Variability of tropical cyclone precipitation volume in the Philippines. International Journal of Climatology, 1–11. https://doi.org/10.1002/joc.7573

Bhatia, K., Vecchi, G., Murakami, H., Underwood, S. & Kossin, J. Projected response of tropical cyclone intensity and intensification in a global climate model. J. Clim. 31, 8281–8303 (2018).

Cha, E. J., Knutson, T. R., Lee, T. C., Ying, M., & Nakaegawa, T. (2020). Third assessment on impacts of climate change on tropical cyclones in the Typhoon Committee Region Part II: Future projections. Tropical Cyclone Research and Review, 9(2), 75-86. https://doi.org/10.1016/j.tcrr.2020.04.005

Cinco, T. A., de Guzman, R. G., Ortiz, A. M. D., Delfino, R. J. P., Lasco, R. D., Hilario, F. D., and Ares, E. D. (2016). Observed trends and impacts of tropical cyclones in the Philippines. International Journal of Climatology, 36(14). https://doi.org/10.1002/joc.4659

Cruz, F. T., Tacan, F. P., Uy, N. T. P., & Santillan, J. R. (2020). Topographical effects on precipitation distribution during typhoons in the Philippines. Natural Hazards, 103(1), 1003-1020.

Da Silva, N.A., Haerter, J.O. Super-Clausius–Clapeyron scaling of extreme precipitation explained by shift from stratiform to convective rain type. Nat. Geosci. 18, 382–388 (2025). https://doi.org/10.1038/s41561-025-01686-4

DeMaria, M., Mainelli, M., Shay, L. K., Knaff, J. A., & Kaplan, J. (2005). Further improvement to the Statistical Hurricane Intensity Prediction Scheme (SHIPS). Weather and Forecasting, 20(4), 531–543. https://doi.org/10.1175/WAF862.1

Delfino, R.J.P., Bagtasa, G., Hodges, K., and Vidale, P.L.V. (2022). Sensitivity of simulating Typhoon Haiyan (2013) using WRF: the role of cumulus convection, surface flux parameterizations, spectral nudging and initial and boundary conditions. Natural Hazards and Earth System Sciences Journal. https://doi.org/10.5194/nhess-22-3285-2022

Delfino, R.J.P., Vidale, P.L., Bagtasa, G., and Hodges, K. (2023). Response of damaging tropical cyclone events in the Philippines to climate forcings from selected CMIP6 models using the pseudo global warming technique. Climate Dynamics. https://doi.org/10.1007/s00382-023-06742-6

Delfino, R.J.P., Hodges, K., Vidale, P.L., and Bagtasa, G., and (2024). Sensitivity of Philippine historically damaging tropical cyclone events to surface and atmospheric temperature forcings. Regional Studies in Marine Science. https://doi.org/10.1016/j.rsma.2024.103595

Formatted: Indent: Left: 0", Hanging: 0.25"

Emanuel, K. (2005). Increasing destructiveness of tropical cyclones over the past 30 years. Nature, 436(7051), 686-688.

Emanuel, K. A. (1987). The dependence of hurricane intensity on climate. Nature, 326(6112), 483-485.

Emanuel, K. A. (1986), An air-sea interaction theory for tropical cyclones. Part I: Steady state maintenance, J. Atmos. Sci., 43, 585–604.

Held, Isaac M., and Brian J. Soden. "Robust responses of the hydrological cycle to global warming." *Journal of climate* 19.21 (2006): 5686-5699.

Hendricks, E. A. M. S., Peng, B. F., & Li, T. (2010). Quantifying environmental control on tropical cyclone intensity change. Monthly Weather Review, 138(8), 3243–3271. https://doi.org/10.1175/2010MWR3185.1

Huprikar, A. S., Stansfield, A. M., & Reed, K. A. (2023). A storyline analysis of Hurricane Irma's precipitation under various levels of climate warming. *Environmental Research Letters*, *19*(1), 014004.

Jiang, H., & Ramirez, E. M. (2013). Necessary conditions for tropical cyclone rapid intensification as derived from 11 years of TRMM data. Journal of Climate, 26(17), 6459–6470. https://doi.org/10.1175/JCLI-D-12-00432.1

Kaplan, J., DeMaria, M., & Knaff, J. A. (2010). A revised tropical cyclone rapid intensification index for the Atlantic and eastern North Pacific basins. Weather and Forecasting, 25(1), 220–241. https://doi.org/10.1175/2009WAF2222280.1

Kaplan, J., Rozoff, C. M., DeMaria, M., Sampson, C. R., Kossin, J. P., Velden, C. S., … Dostalek, J. F. (2015). Evaluating environmental impacts on tropical cyclone rapid intensification predictability utilizing statistical models. Weather and Forecasting, 30(5), 1374–1396. https://doi.org/10.1175/WAF-D-15-0032.1

Knutson, T. R. et al. Global projections of intense tropical cyclone activity for the late twenty-first century from dynamical downscaling of CMIP5/RCP4.5 scenarios. J. Clim. 28, 7203–7224 (2015).

Knutson, T. R., McBride, J. L., Chan, J., Emanuel, K., Holland, G., Landsea, C., ... & Sugi, M. (2010). Tropical cyclones and climate change. Nature Geoscience, 3(3), 157-163.

Knutson, T. R., McBride, J. L., Chan, J., Emanuel, K., Holland, G., Landsea, C., ... & Sugi, M. (2008). Tropical cyclones and climate change. Nature Geoscience, 1(3), 157-163.

Kossin, J. P., Emanuel, K. A., & Vecchi, G. A. (2017). The poleward migration of the location of tropical cyclone maximum intensity. Nature, 509(7500), 349-352.

Lau, W. K. M. & Zhou, Y. P. Observed recent trends in tropical cyclone precipitation over the North Atlantic and the North Pacific. J. Geophys. Res. 117, D03104 (2012).

Lenderink, G., R. Barbero, J. M. Loriaux, and H. J. Fowler, 2017: Super-Clausius–Clapeyron Scaling of Extreme Hourly Convective Precipitation and Its Relation to Large-Scale Atmospheric Conditions. *J. Climate*, **30**, 6037–6052, https://doi.org/10.1175/JCLI-D-16-0808.1.

Liu, M., Vecchi, G.A., Smith, J.A. et al. Causes of large projected increases in hurricane precipitation rates with global warming. npj Clim Atmos Sci 2, 38 (2019). https://doi.org/10.1038/s41612-019-0095-3

Macalalad R, Delfino RJP, Badilla RA, Paat SF and G Bagtasa (2023). Role of Historical Warming on the Extreme Flooding Event Due to Typhoon Vamco (Ulysses) 2020 in the Philippines. Philipp J Sci 152(S1): 197–212.https://philjournalsci.dost.gov.ph/publication/special-issues/meteorology/121-vol-152-no-s1-

meteorology/1973-role-of-historical-warming-on-the-extreme-flooding-event-due-to-typhoon-vamco-ulysses-2020-in-the-philippines

Montgomery, Michael T., John Persing, and Roger K. Smith. "Putting to rest WISHE-ful misconceptions for tropical cyclone intensification." *Journal of Advances in Modeling Earth Systems* 7, no. 1 (2015): 92-109.

O'Gorman, P. A. (2020). Precipitation extremes in a warming climate. Annual Review of Climate Science, 1, 41-63.

Pendergrass A G and Hartmann D L 2014 Two modes of change of the distribution of rain J. Clim. 27 8357–71

Rotunno, R., and K. A. Emanuel (1987), An air-sea interaction theory for tropical cyclones. Part II: Evolutionary study using a nonhydrostatic axisymmetric numerical model, J. Atmos. Sci., 44, 542–561.

Ruan, Z., & Wu, Q. (2018). Precipitation, convective clouds, and their connections with tropical cyclone intensity and intensity change. Geophysical Research Letters, 45(2), 1098-1105.

Shi, X., Liu, Y., Chen, J. et al. Escalating tropical cyclone precipitation extremes and landslide hazards in South China under Global Warming. npj Clim Atmos Sci 7, 107 (2024). https://doi.org/10.1038/s41612-024-00654-w

Trenberth, K. E., Dai, A., Rasmussen, R. M., & Parsons, D. B. (2003). The changing character of precipitation. Bulletin of the American Meteorological Society, 84(9), 1205-1217.

Stansfield, A.M., Reed, K.A. Global tropical cyclone precipitation scaling with sea surface temperature. *npj Clim Atmos Sci* **6**, 60 (2023). https://doi.org/10.1038/s41612-023-00391-6

Sun, Ying, et al. "How often will it rain?." Journal of Climate 20.19 (2007): 4801-4818.

Tao, C., & Jiang, H. (2015). Distributions of shallow to very deep precipitation-convection in rapidly intensifying tropical cyclones. Journal of Climate, 28(22), 8791–8824. https://doi.org/10.1175/JCLI-D-14-00448.1

Tierra, M.C.M. and Bagtasa, G., (2023). Identifying the rapid intensification of tropical cyclones using the Himawari-8 satellite and their impacts in the Philippines. International Journal of Climatology, 43(1), pp.1-16.

Trenberth, K. E., Dai, A., Rasmussen, R. M., & Parsons, D. B. (2003). The changing character of precipitation. Bulletin of the American Meteorological Society, 84(9), 1205-1217.

Trenberth, K. E., Zhang, Y., & Fasullo, J. T. (2007). Global warming and the hydrologic cycle. Journal of Climate, 20(17), 3589-3610.

Trenberth, K. E. (2009). Precipitation in a changing climate-more floods and droughts in the future. *Gewex News*, *19*(May 2009), 8-10.

Vecchi, G. A. et al. Tropical cyclone sensitivities to CO2 doubling: roles of atmospheric resolution, synoptic variability and background climate changes. Clim. Dyn. https://doi.org/10.1007/s00382-019-04913-y (2019).

Vecchi, G. A., Soden, B. J., Wittenberg, A. T., Held, I. M., Leetmaa, A., & Harrison, M. J. (2008). Weakening of tropical Pacific atmospheric circulation due to anthropogenic forcing. Nature, 441(7089), 73-76.

Wang, S., Nie, J., Evans, J. P., & Zhu, X. (2019). Super Clausius–Clapeyron scaling of extreme hourly convective precipitation and its relation to large-scale atmospheric conditions. Geophysical Research Letters, 46(11), 6122-6131.

Yamada, Y., M. Satoh, M. Sugi, C. Kodama, A. T. Noda, M. Nakano, and T. Nasuno, 2017: Response of Tropical Cyclone Activity and Structure to Global Warming in a High-Resolution Global Nonhydrostatic Model. J. Climate, 30, 9703–9724, https://doi.org/10.1175/JCLI-D-17-0068.1.

Yoshida, K., Sugi, M., Mizuta, R., Murakami, H. & Ishii, M. Future changes in tropical cyclone activity in high-resolution large-ensemble simulations. Geophys. Res. Lett. 44, 9910–9917 (2017).

Xi, D., Wang, S., & Lin, N. (2023). Analyzing relationships between tropical cyclone intensity and rain rate over the ocean using numerical simulations. Journal of Climate, 36(1), 81-91. https://doi.org/10.1175/JCLI-D-22-0141.1

SUPPLEMENTARY MATERIAL

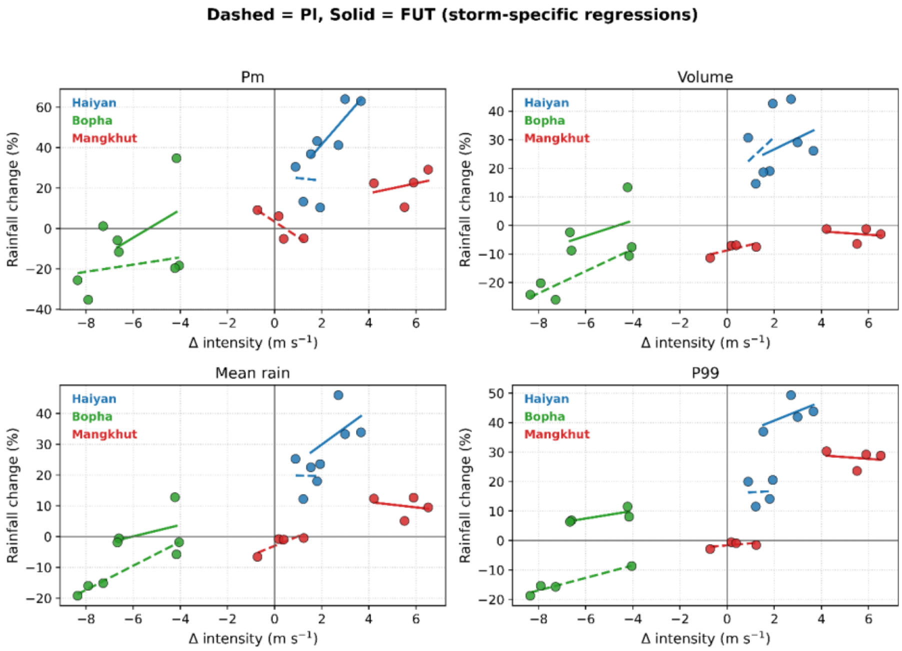

Supplementary Figure 1. Relationship between changes in tropical cyclone intensity (Δ intensity, m s^{-1}) and rainfall response for preindustrial (dashed lines) and future (solid lines) simulations. Panels show percent changes in azimuthally averaged maximum rainfall rate (Pm), rainfall volume, mean rainfall rate, and extreme rainfall (P99). Solid lines indicate linear fits for each climate state, highlighting a stronger and more consistent positive scaling between intensity and rainfall under future warming compared to preindustrial conditions